COMPARISON OF SUBSTRATE CONDITIONS IN LOW-TEMPERATURE GALLIUM ARSENIDE AND SEMI-INSULATING GALLIUM ARSENIDE DURING TERAHERTZ PULSE GENERATION

A Thesis

Presented to

the Faculty of the Graduate School

at the University of Missouri-Columbia

In Partial Fulfillment

of the Requirements for the Degree

Master of Science

---

by

ARUN KUMAR ALLA

Dr. Naz E. Islam, Thesis Supervisor

JULY 2011

The undersigned, appointed by the dean of the Graduate School, have examined the thesis entitled

COMPARISON OF SUBSTRATE CONDITIONS IN LOW-TEMPERATURE GALLIUM ARSENIDE AND SEMI-INSULATING GALLIUM ARSENIDE DURING TERAHERTZ PULSE GENERATION

Presented by Arun Kumar Alla

A candidate for the degree of Master of Science

And hereby certify that, in their opinion, it is worthy of acceptance.

Professor N. E. Islam, Dept. of Electrical and Computer Engineering

---

Professor Mahmoud Almasri, Dept. of Electrical and Computer Engineering

---

Professor Sashi Satpathy, Dept. of Physics and Astronomy

ACKNOWLEDGEMENTS

First and foremost I offer my sincerest gratitude to my supervisor, Dr. Naz Islam, who has supported me throughout my thesis with his patience and knowledge whilst allowing me the room to work in my own way. I attribute the level of my Masters degree to his encouragement and effort and without him this thesis, too, would not have been completed or written. I could not have imagined having a better advisor and mentor for my master's study.

I gratefully thank Dr. Mahmoud Almasri and Dr. Sashi Satpathy for their constructive comments on this thesis. I am thankful that in the midst of all their activity, they accepted to be members of the reading committee.

Finally, I would like to thank my parents, colleagues, friends and everybody who was important to the successful realization of thesis, as well as expressing my apology that I could not mention personally one by one.

Table of Contents

Acknowledgements ii

List of Figures v

Abstract vii

Chapter 1: Introduction 1

1.1 Terahertz (THz) radiation 1

1.2 Terahertz (THz) radiation Applications 4

1.3 Overview of the Thesis 4

Chapter 2: Background 6

2.1 Photoconductive Switch Definition 6

2.2 Photoconductive Switch Fundamentals 6

2.3 Functioning of Photoconductive Switch 7

2.4 Linear Photoconductive Switch Parameters 8

2.5 Classification of Photoconductive Semiconductor Switches 10

2.6 Types of Photoconductivity 13

2.7 Photoconductive Semiconductor Switch Materials 13

2.8 Low-Temperature Gallium Arsenide (LT-GaAs) 15

2.9 Semi-Insulating Gallium Arsenide (SI-GaAs) 16

Chapter 3: Literature Survey 19

Chapter 4: Device Simulation 26

4.1 Silvaco Software 26

4.1.1 ATLAS 26

4.2 Nonlinear Equations 31

4.3 Carrier Generation – Recombination Models 32

4.4 Impact Ionization Models 33

4.5 Band-to-Band Tunneling 34

4.6 Non-Linear Iteration 35

4.7 Traps and Defects in Semiconductors 35

4.8 Parameters used in the simulation 37

4.9 Mesh Simulation 38

Chapter 5: Results and Discussion 40

5.1 PCSS Devices Studied 40
5.1.1 Semi-Insulating Gallium Arsenide (SI-GaAs) PCSS 40
5.1.2 Low-Temperature Gallium Arsenide (LT-GaAs) PCSS 42

5.2 Simulation Results and Discussion 44
5.2.1 Analysis of I-V Characteristics 44
5.2.2 Analysis of Recombination Rate 45
5.2.3 Analysis of Total Current Density 48
5.2.4 Analysis of On State Response 52

Chapter 6: Conclusion 55

6.1 Summary of Work 55

References 58

Appendix 65

LIST OF FIGURES

Figure 1. 1 Terahertz frequency occupies a portion of electromagnetic spectrum in between the infrared and microwave radiation 2

Figure 1. 2 Terahertz frequency generation from photoconductive semiconductor switch when illuminated with femtosecond laser 3

Figure 2. 1 Illustration of Photoconductive Switch Ref[35]. 7

Figure 2. 2 Lateral PCSS configuration 11

Figure 2. 3 Vertical PCSS configuration 12

Figure 2. 4 Various Compensation Structures in Semi-Insulating Gallium Arsenide 16

Figure 3. 1 Experimental test n-i-n structure Ref[13] 21

Figure 3. 2 Low-Temperature Gallium Arsenide photoconductive antenna for THz generation and detection Ref[19] 23

Figure 3. 3 Schematic sketch of the THz emitting MSM structure [23] 23

Figure 4. 1 Atlas Inputs and Outputs 28

Figure 4. 2 ATLAS Command Groups with the Primary Statements in each group 28

Figure 4. 3 Definition of the trap energy level for acceptor and donor traps in reference to the conduction and valance band edges 36

Figure 4. 4 Simulation Mesh 38

Figure 5. 1 Semi-Insulating Gallium Arsenide (SI-GaAs) PCSS 41

Figure 5. 2 Low-Temperature Gallium Arsenide (LT-GaAs) PCSS 43

Figure 5. 3 I-V Characteristics of LT-GaAs PCSS and SI-GaAs PCSS 45

Figure 5. 4 Recombination Rate Profile of both PCSS at 120V 46

Figure 5. 5 Recombination Rate Profile of both PCSS at 250V 47

Figure 5. 6 Overlay of Recombination Rate contour profile with time before (t=0 fs), immediately at the end of laser pulse (t=80 fs) of both SI-GaAs and LT-GaAs PCSS respectively at 250V 48

Figure 5. 7 Total Current Density Profile of both PCSS at 120V..... 50

Figure 5. 8 Total Current Density Profile of both PCSS at 250V..... 50

Figure 5. 9 Total Current Density contour profile with time before (t=0 fs), immediately at the end of laser pulse (t=80 fs) of both SI-GaAs, and LT-GaAs PCSS respectively..... 51

Figure 5. 10 Total Current Density vector profile with time before (t=0 fs), immediately at the end of laser pulse (t=80 fs) of both SI-GaAs, and LT-GaAs PCSS respectively..... 51

Figure 5. 11 On State Response of SI-GaAs PCSS and LT-GaAs PCSS at 120V and 250V respectively..... 53

ABSTRACT

The use of GaAs photoconductive semiconductor switches (PCSS) for generating THz radiation is well known. Both semi-insulating (SI) and Low-temperature (LT) grown Gallium Arsenide (GaAs) have been used. In this research the material parameters that affects the generated pulse shape is studied and compared. Specifically, the role of traps, its density and concentration, carrier rise time, beam width and decay have been analyzed. An industry standard simulation suite was used in the analysis.

Study shows that for both LT-GaAs and SI-GaAs there is an increase in total current density with the application of higher bias voltage. Increase in bias increased the drift component through velocity and depletion width increase. Since SI-GaAs have a relatively larger trap concentration at midgap than LT-GaAs and the carrier recombination rate is also higher in SI-GaAs, the linearity the collected charge plot of SI-GaAs is more affected than that of LT-GaAs PCSS. Consequently, charge collection and rise time is faster in LT-GaAs based PCSS as compared to SI-GaAs and will thus transfer more energy to the load that SI based PCSS. The both LT-GaAs PCSS and SI-GaAs PCSS, the role of traps is an important factor that determines the generated pulse shape and width. Specifically effects of recombination rate, beam width and decay and carrier rise time influences the current density and the shape of THz pulse generated. Further, it was observed that LT-GaAs based photoconductive semiconductor switches have superior resistivity (breakdown fields) and charge collection values when compared to SI-GaAs based photoconductive semiconductor switches.

CHAPTER 1: INTRODUCTION

This chapter provides an overview of the different techniques employed in generating Terahertz (THz) radiation and its application in many fields. .

1.1 Terahertz (THz) radiation

Since the last two decades there has been intense research on semiconductor photoconductor devices in the development of picosecond and subpicosecond electrical signal generation motivated by the fast – growing demand for ultrafast, integrated optoelectronic photoswitches and photodetectors. There has been a development of efficient emitters and detectors within each of the spectral regions in the electromagnetic spectrum that has resulted in the birth of several industries. Because of the development of femtosecond pulsed lasers, several techniques have been applied to generate and detect the terahertz pulsed radiation, which is a very fast growing field and has extremely high potential for applications in academic research, defense and in industry.

The term “Terahertz radiation” is derived from the frequency of radiation of the order of one trillion oscillations per second. The Terahertz region in electromagnetic spectrum is defined in the frequency range from 0.1 to 10 THz and it lies between infrared and microwave radiation as shown in Figure 1.1.

THz sources employing semiconductors include the use of the material surfaces [14], optical rectification [7], and fast-closing photoconductive semiconductor switch (PCSS) [6]-[8]. Of the many methods used in the generation of THz radiation, the most

prominent and well known method is the use of the photoconductive semiconductor switches (PCSS).

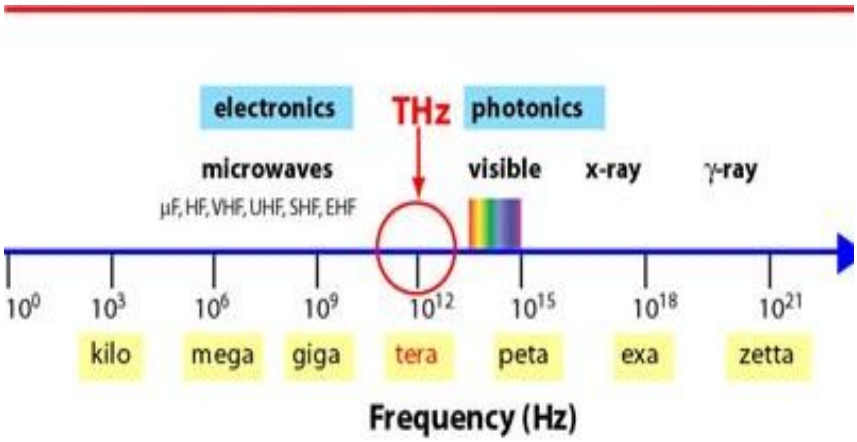

Figure 1. 1 Terahertz frequency occupies a portion of electromagnetic spectrum in between the infrared and microwave radiation

Semiconductor based THz system is basically made up of a source generator which is intimately attached to a THz radiator. The PCSS, which are excited through femtosecond (fs) lasers, provides a much better intensity and spectral bandwidth. The radiation from the PCSS is initiated when the gap between the contacts of the PCSS is illuminated with an optical pulse; the duration of the illumination is less than the desired frequency of operation. As shown in Figure 1.2, when a femtosecond laser pulses illuminates the surface of the photoconductive semiconductor switches, the photon energies that exceed the semiconductor bandgap create electron – hole pairs or carriers that take part in the conduction processes. If there is an applied field across the PCSS the photo generated

free charge carriers are accelerated which results in terahertz generation. The intensity of THz radiation is proportional to the time derivative of the transient current.

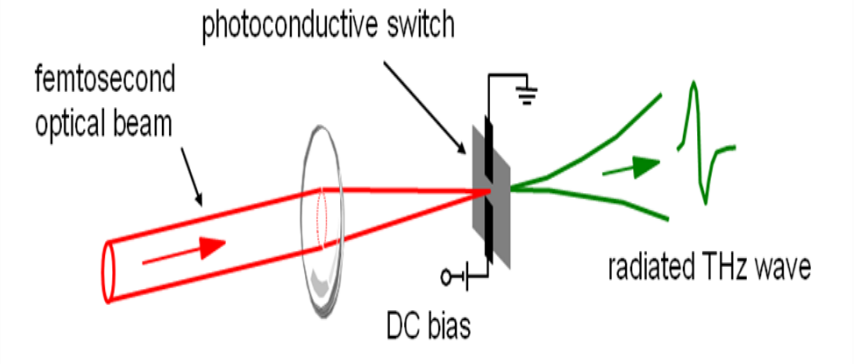

Figure 1. 2 Terahertz frequency generation from photoconductive semiconductor switch when illuminated with femtosecond laser

The Semiconductor materials having high dielectric-breakdown fields or wide band-gap semiconductors such as Silicon Carbide (SiC) and Gallium Nitride (GaN) are used as the PCSS material; apart from these materials the GaAs provides very promising results thus can be used for PCSS generating THz radiation. Both SiC and GaN has a limitation with the carrier lifetime but it shows significant improvement in the power of the generated radiation.

It has been stated earlier about the advances in the experimental development of the Terahertz systems [8], but the same kind of advancement is not found in the literature about the integrated source - radiator system analysis which specifically uses the photoconductive semiconductor switch (PCSS). A lot of advancement has been made in the study of photoconductive semiconductor switches in Terahertz regime but there has

been no comprehensive and comparative study of the GaAs photoconductive semiconductor switches. This research is an attempt to fill this gap.

1.2 Terahertz (THz) radiation Applications

Due to the fast growing field of Terahertz (THz) radiation, many applications have been found in many fields. Applications include areas of cellular level imaging and chemical, biological sensing, space tomography etc. Material characteristics can be analyzed and their parameters extracted at frequencies which is not practical at other frequency bands. Thus applications in space, commercial and defense sectors, label – free genetic analysis, high – temperature superconductor characterization, real – time two dimensional and three dimensional terahertz frequency computed tomography is possible using THz radiation. THz radiation is also used to characterize materials for various applications; specifically to manipulate and control quantum mechanical states in matter. High power terahertz (THz) sensors have higher resolution than existing RF and microwave sensors. Terahertz radiation can be used to differentiate varying degrees of water content in materials because of its high absorption in water. THz can also be used for detecting explosive materials. In the field of semiconductors, terahertz technology has had an impact on the fundamental limits of electronic devices, quantum mechanics, quantum information science, spintronics, and subwavelength THz spectroscope.

1.3 Overview of the Thesis

In this thesis work, the substrate conditions and characteristics of Low – Temperature gallium Arsenide and Semi –Insulating Gallium Arsenide photoconductive semiconductor switches during Terahertz (THz) pulse generation. Following this

introductory chapter on THz radiation and its applications, the thesis is organized as follows: Chapter 2 briefly describes the background of the basic operation of photoconductive semiconductor switches used in the research work, and the different semiconductor materials used for the PCSS for terahertz pulse generation and their properties are also presented.

Chapter 3 explains the previous work done which have had a strong influence on the present research work, and also gives the literature survey for this thesis work.

Chapter 4 briefly explains the mathematical models and equations used for the study presented, and also describes the simulation software tool used in this research work.

Chapter 5 briefly explains the simulation results and analysis of the results as well as the characteristics of LT-GaAs PCSS and SI-GaAs under different bias voltages is presented.

Chapter 6 presents the summary of the work and also the possible future work in this area of research.

CHAPTER 2: BACKGROUND

This chapter presents the background of the photoconductive semiconductor switches and its operation. It also describes the different semiconductor materials used for PCCS for terahertz pulse generation and their properties.

2.1 Photoconductive Switch Definition

A photoconductive semiconductor switch or PCSS is defined as an electrical switch which is based on the photoconductivity of the material. That is, due to its high resistivity (> 10^9 Ω-cm) the material is in the non-conducting or 'off' state when a bias is applied across it. However when a laser beam with photon energy larger than the bandgap of the material irradiation the switch, current conduction takes place and the PCSS is in the 'on' state due to the creation and collection of charge.

2.2 Photoconductive Switch Fundamentals

The fundamental optically controlled semiconductor (or photoconductive) switch is used to connect a source to a load. The photoconductive switch shown in Figure 2.1 consists of two electrical contacts which are separated by a semiconductor material medium of length h_s, width w_s, thickness d_s. To make sure all the optical energy is being absorbed by the bulk semiconductor material, the thickness d_s should be greater than or equal to the optical absorption length d_o. The distance between the electrical contacts h_s is determined by the required operating voltage.

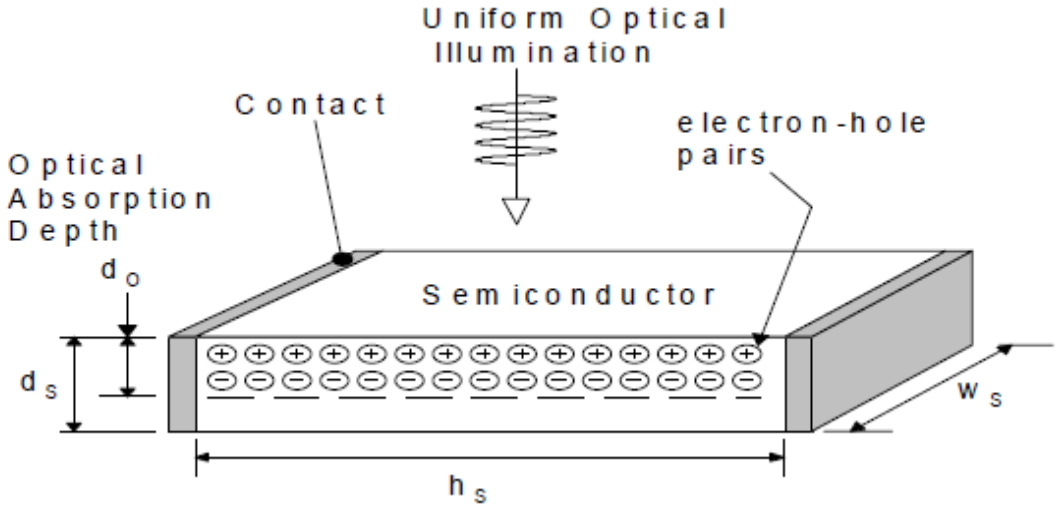

Figure 2. 1 Illustration of Photoconductive Switch Ref[35].

$$h_s = \frac{V_s}{E_s} \tag{2.1}$$

Where, V_s is the voltage across the switch, E_s is the average electric field across the switch. The width w_s are determined by the desired thermal resistance from the switch to the surrounding medium. With the illumination of uniform optical intensity source between the contacts change the planer, insulator, photoconductive medium to conductor.

2.3 Functioning of Photoconductive Switch

There are two fundamentals steps in the working of the photoconductive switch. One state is the on state known as avalanche injection state and the other state is the off state known as blocking state.

---On (Avalanche Injection) State

Impact ionization results in a two-carrier conduction state under breakdown conditions when the peak field in the device exceeds the avalanche breakdown field.

Breakdown of the switch occurs when the applied voltage is lower than the breakdown voltage, optical triggering will generate electron-hole pairs [20].

$$J = qE(x)\left[\mu_n n(x) + \mu_p p_n\right] \tag{2.2}$$

$$\frac{\varepsilon}{q}\frac{dE}{dx} = n(x) - p_n + N_a \tag{2.3}$$

Where p_n is background hole density, N_a is shallow acceptor density, ε is dielectric constant of the semiconductor material

--- Off (Blocking) State

In this state a small amount of current flows through the photoconductive switch. The equations for steady-state conduction given below [20]:

$$J = qvn(x) \tag{2.4}$$

$$\frac{\varepsilon}{q}\frac{dE(x)}{dx} = n(x) - N_d^+ + N_a^- - N_t^+ \tag{2.5}$$

$$\frac{dJ}{dx} = -q\left[G(x) - R(x)\right] \tag{2.6}$$

Where q is unit elementary charge, ε is dielectric constant of the semiconductor material J is current density, E(x) is electric field intensity, v is drift velocity, n(x) is ionized trap density, N_t^+ is ionized deep donor density

2.4 Linear Photoconductive Switch Parameters

There are two parameters in the linear photoconductive switch: one parameter is the on state resistance and other parameter is the off state resistance.

--- Off state Resistance

The dark or steady state resistivity of the semiconductor slab, ρ_o determines the open or off state resistance, R_{so}, of the switch. The equation as follows [35]:

$$R_{so} = \frac{\rho_0 . h_s}{w_s . t_s} \tag{2.7}$$

This will naturally lead to the requirement that the semiconductor material be intrinsic or compensated such that the dark resistivity is large and the corresponding open resistance is large.

--- On state Resistance

When the optical energy is applied to the surface of the semiconductor, the resistance of the photoconductive switch decreases. The switch on (conduction) resistance related to the conductivity through the switch geometry is given by equation as follows [35]:

$$R_{sc} = \frac{h_s}{\sigma_s . w_s . d_o} = \frac{\varepsilon_\lambda . h_s^2}{q_e . \mu_s . E_o (1 - S_r)} \tag{2.8}$$

Where h_s is length of the switch, ε_λ is photon energy, q_e is electron charge, E_o is optical energy incident on the switch surface, μ_s is sum of hole and electron mobilities and S_r is surface optical reflection coefficient.

The switch waveform follows the light pulse when the time resolution of the pulse is greater than the recombination time T_r.

$$R_{sc} = \frac{\varepsilon_\lambda . h_s^2}{q_e . \mu_s . T_r . E_o (1 - S_r)} \tag{2.9}$$

A linear photoconductive switch is desirable because the conduction resistance, the current density, and the conduction time can be determined by controlling the optical pulse source and the material recombination time.

2.5 Classification of Photoconductive Semiconductor Switches

The photoconductive semiconductor switches are classified into two categories: 1) According to mode of operation 2) According to geometry

1) According to mode of operation

--- Linear Mode Photoconductive Semiconductor Switch

When one electron hole pair is produced, each photon absorbed is characterized as linear mode. The switch conductivity approximately follows the amplitude of the optical drive pulse where the conductivity of the material is, to first order, linearly proportional to the total photon flux illuminating the semiconductor material. The switch closes as the optical intensity increases, remains closed while illuminated, and opens with characteristic time constants related to the carrier lifetimes once the optical pulse is removed. The rise time of the electric pulse is determined by the speed of the laser and fall time is determined by material properties related to carrier life time.

--- Nonlinear Mode Photoconductive Semiconductor Switch

When the bias electric field in Gallium Arsenide across the switch exceeds approximately 4 to 8 kV/cm, a transition occurs to a nonlinear mode that exhibits high–gain and extended conduction. This is referred to as lock-on [36]. In lock-on, if the laser pulse is strong enough, determine the closing time of the switch, as in linear mode, but the switch then remains closed or locked-on until the current is interrupted by the circuit.

The turn-on speed of the switch is determined by the avalanche process independent of the laser time when the nonlinear electric field threshold for GaAs is reached. The optically generated carriers can dominate and switch turn-on is faster than its characteristic avalanche time when the laser rise time is faster than the avalanche rise time and the laser amplitude is high enough. The switch still locks on even though the optical pulse from the laser may have ended.

Trap filling and impact ionization of traps are among the possible explanations [37, 38] for the mechanisms leading to avalanche-like rise and lock-on nonlinear switching behavior.

2) According to geometry

--Lateral PCSS

The lateral PCSS geometry is shown in Figure 2.2

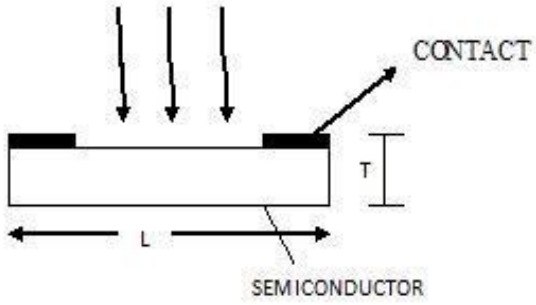

Figure 2. 2 Lateral PCSS configuration

This is the simplest design to couple optical energy into the switch. It is easy to understand and diagnose. All the light is absorbed in the active region of the switch whether it is absorbed in a few micrometers or several hundred micrometers. For a

uniformly illuminated, lateral, linear switch, the peak current and the rise time depend only on the magnitude and shape of the optical pulse, the carrier recombination time, and the configuration of the switch in an external circuit. Exposure of the wafer surface to the maximum electric field is the disadvantage of the later switch geometry. Electrical breakdown is usually significantly lower than the bulk electrical breakdown strength of the semiconductor material. The transit time or space charge limited current flow is not an issue.

--Vertical PCSS

The vertical PCSS is shown in Figure 2.3

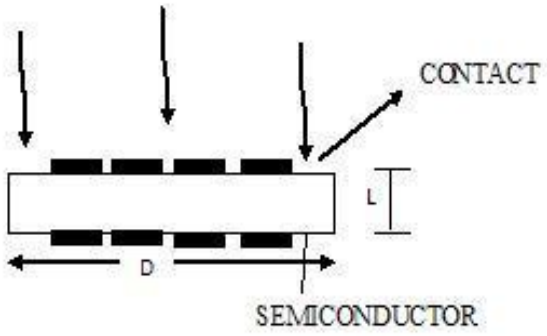

Figure 2. 3 Vertical PCSS configuration

The vertical PCSS configuration increases the voltage hold-off (level of voltage it can sustain before breaking down) of a PCSS by reducing fields near the switch surfaces. The main obstacle to this configuration is that, atleast one of the electrical contacts to the switch must be transparent to the optical trigger. The way to overcome this problem is to use metallic grid, very thin metallic layers, or epitaxially grown, doped semiconductor layers. The absorption depth of the optical trigger plays an important role. Careful tuning

of the trigger wavelength to the switch thickness might optimize the switching efficiency and risetimes, but different materials would be required to produce different size switches to handle different peak voltages.

2.6 Types of Photoconductivity

Photoconductivity is of two types:

1) Intrinsic Photoconductivity: If the photon energy is greater than the band gap.
2) Extrinsic Photoconductivity: If the photon energy is less than the band gap if the traps are used to generate the free carriers.

Photoconductive semiconductor switches are used in several purposes:

a) Testing of high-speed integrated electronic circuits
b) Generation of terahertz pulses
c) Generation of microwaves and millimeter waves via direct DC and RF conversion, in both continuous-wave and pulsed mode
d) In very fast analog-to-digital converters

2.7 Photoconductive Semiconductor Switch Materials

Semiconductors are classified, based on the response of the material to majority carrier injection, as a relaxation type and lifetime type. The Debye length is much greater than the diffusion length in case of relaxation type behavior materials, the injection of majority carriers leads to majority carrier depletion. In lifetime type materials, if the diffusion length is much greater than the Debye length, then the injection of majority carriers leads to majority carrier augmentation. The resistivity in semiconductors varies inversely as the free carrier concentration, both intrinsic and compensated (with high

density of trap levels near the mid-gap) semiconductors [30, 31] having low free carrier concentrations are high materials. In intrinsic semiconductors and compensated semiconductors the charge transport differs. The charge transport characteristics is better in compensated materials because their properties are similar to lifetime materials where the diffusion length is much greater than the Debye length and comparable to majority carrier lifetime thus increase the performance of the Photoconductive semiconductor switch as a whole. The charge transport characteristics are poor in intrinsic materials compared to compensated materials because their properties of relaxation type materials where the Debye length are much greater than the diffusion length and comparable to the minority carrier lifetime thus affecting the performance of the photoconductive semiconductor switch as a whole.

The compensated materials are made through various growth techniques such as liquid encapsulated Czechoraski (LEC), horizontal Bridgeman (HB) mechanism, vertical gradient freeze (VGF) as well as some other methods [30]. Even though any two compensation techniques may give the same value of the material resistivity, the various impurity types and trap levels might affect the conduction properties of the photoconductive semiconductor switches. In order to study and understand the device rise time and lifetime, it is important to look into the material type, compensation processes and resistivity of the material.

Two compensated semiconductor materials are used for photoconductive semiconductor switch for terahertz pulse generation. The two compensated semiconductor materials are Low-Temperature Gallium Arsenide and Semi-Insulating Gallium Arsenide.

2.8 Low-Temperature Gallium Arsenide (LT-GaAs)

Low-Temperature grown GaAs (LT-GaAs) is GaAs grown at a temperature of $200 – 300^0$, usually with a slight excess of Arsenic. The properties of LT-GaAs depend on the degree of post-growth annealing. It can be produced with high resistivity and with subpicosecond carrier life time, which makes it ideal for ultrafast photodetectors that are based on displacement current. In that category of device, the response time is limited by the recombination lifetime of photogenerated carriers. It has been observed that operating these devices under high bias conditions tends to increase the response time.

The important property of LT-GaAs is its specific conductivity which decreases tremendously after an anneal at 600^0 C for 10 to 30 minutes. Annealed LT-GaAs has resistivity of $10^6 – 10^7$ Ωcm compared to about 10Ωcm for normally grown GaAs and 10^5 Ωcm for semi-insulating (SI) GaAs substrates. During the annealing step, the excess arsenic is coalescing to precipitates, the material relaxes and the lattice constant recovers to the value of normal MBE-grown GaAs. In annealed LT-GaAs metal-like clusters of arsenic act like buried Schottky barriers. When the number of these precipitates is high enough, the depletion regions will overlap and the material in between the As-clusters becomes highly resistive [40, 41]. The As-grown material has a resistivity of $10\text{-}10^2$ Ωcm, which increases as a function of the anneal temperature to $10^6 – 10^7$ Ωcm for an anneal at 600^0 C for 10 minutes.

The second important characteristic of low temperature grown GaAs material is the (sub) picosecond carrier lifetime. This characteristic has a strong impact on the fabrication of ultrafast MSM-type photodetectors. The carrier lifetime of LT-GaAs is obtained by measuring the transient reflectivity. The lifetime decreases with decreasing

growth temperature. When the material is grown above 300^0 C, the carrier lifetime is strongly increasing towards the radiative carrier lifetime of normal GaAs of 1ns. The carrier lifetime below this temperature is about 0.25-0.3 ps [15].

2.9 Semi-Insulating Gallium Arsenide (SI-GaAs)

If EL2 is present in GaAs, the semi-insulating behavior can be obtained. The EL2 energy is an electron trap found in GaAs. There are three compensation structures in Semi-Insulating Gallium Arsenide. They are Deep Donors Shallow Acceptors (DDSA), Shallow Donor and Deep Acceptor (SDDA), and Deep Donor Deep Acceptor (DDDA) as shown in Figure 2.4.

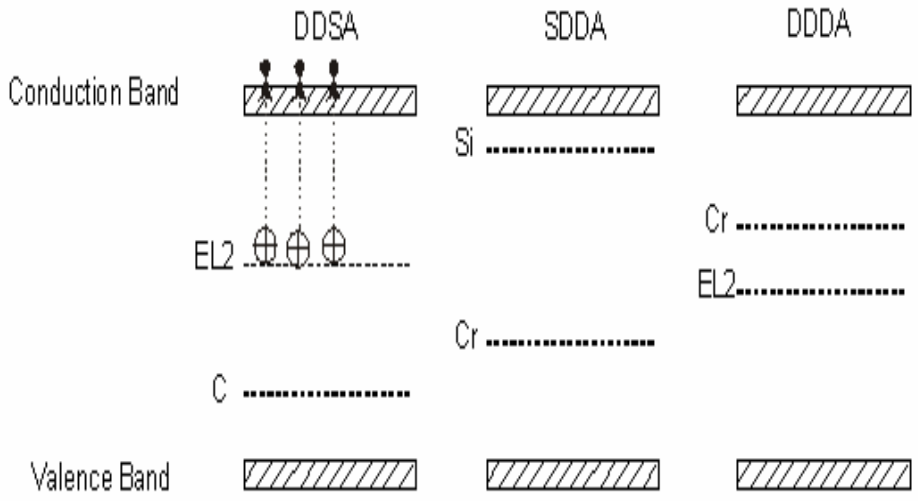

Figure 2. 4 Various Compensation Structures in Semi-Insulating Gallium Arsenide

The balance is obtained between the deep lying EL2 and shallow acceptor impurity, generally carbon, in the Deep Donor Shallow Acceptor (DDSA) compensation structure scheme. This type of material is grown by Liquid-Encapsulated Czochralski (LEC)

technique. The balance is obtained between Chromium (Cr) deep level acceptors and Silicon (Si) Shallow donors in Shallow Donor Deep Donor (SDDA) compensation structure scheme. This type of material is grown by Horizontal Bridgman (HB) technique. The EL2 is compensated by Chromium (Cr) deep acceptors in Deep Donor Deep Acceptor compensation structure scheme. More information is found in references [43]-[46].

The Deep Donor Shallow Acceptor mechanism for Semi-Insulating GaAs behavior is the compensation of EL2 by carbon acceptors [47, 48]. The ionization of EL2 produces an ionized center plus an electron in the conduction band

$$\text{Unionized EL2} \rightarrow \text{Ionized EL2} + e^- \tag{2.10}$$

According to the mass action law, the relation between the concentration of ionized centers N_I, the concentration of electrons n, and the concentration of unionized centers N_U are given by the equation:

$$\frac{N_{I^n}}{N_U} = K \tag{2.11}$$

Where K is a constant determined by the thermodynamics of the system, N_I is equal to the net acceptor concentration, given as the difference in concentration between shallow acceptors N_A and shallow donors N_D

$$N_I = N_A - N_D \tag{2.12}$$

The concentration of acceptors is given as the sum of the concentrations of carbon and other residual acceptors N_A^R.

$$N_A = [\text{carbon}] + N_A^R \tag{2.13}$$

The concentration of neutral centers is equal to the EL2 concentration as determined by optical absorption. That is, only EL2 centers that are occupied by electrons contribute to the optical absorption process.

$N_U = [EL2]$ (2.14)

We rearrange the above equations

$$n = K\frac{[EL2]}{[carbon] + N_A^R - N_D} \quad (2.15)$$

The above equation can be written as

$$[carbon] = K\frac{[EL2]}{n} + N_D - N_A^R \quad (2.16)$$

Therefore, the carbon concentration is proportional to the ratio of the EL2 concentration to the electron concentration. EL2 deep donors and carbon shallow acceptors control the electrical compensation in semi-insulating LEC grown GaAs.

Semi-Insulating Gallium Arsenide exhibits better rise time, jitter characteristics, and high resistivity.

CHAPTER 3: LITERATURE SURVEY

Photoconductive switches made from Semi-Insulating Gallium Arsenide were proposed in the late 1970's for use of both closing and opening high-power switches [1]. Closing was achieved by exciting electrons from the valence band into the conduction band using a laser with photon energy greater than that of the band gap. An alternative method to direct excitation across the bandgap was proposed by Schoenbach, et al. [2]. This concept, which is called the Bistable Optically controlled Semiconductor Switch (BOSS), relies on persistent photoconductivity followed by photo-quenching to provide both switch closing and opening [3]. K. Horio et.al [4] presented the electrical properties of Low-Temperature Gallium Arsenide using an n-i-n structure. The I-V curve showed three distinct regions and observed slow trapping-detrapping of electrons with a time scale of 1~10 seconds. This model can further be used in simulations of electrical device structures which incorporate LT-GaAs. About 10 years ago, a paper was written by Williams [5] proposing a method for generating large amount of terahertz light. Williams started following the development of JLab's free –electron laser. Williams and his collaborators presented their results at the First International Conference on Terahertz Radiation in December of 2001. Due to the novel arena, the U.S. Navy funded the FEL's to investigate the high-power laser beams whose precise wavelength can be selected. The possibility of generating a microwave replica of a picosecond optical pulse is particularly attractive. Recently, a simple method for generating a microwave replica of picosecond optical pulse has been demonstrated. Using a light-activated photoconductive switch to

drive a X-band waveguide, a microwave pulse shorter than 50 psec and accurately synchronized with the optical driving pulse was observed. In this letter reported an extension of this technique to produce even shorter microwave bursts by means of a subpicosecond laser driving a GaAs photoconductive switch [6]. In 1988 a publication D. Auston et.al [7] presented that the electrooptic Cherenkov effect is an effective method of generating extremely short electrical pulses for use in applications for the measurement of the static and dynamical properties of materials in the FIR. Peter R. Smith et.al [8] demonstrated that photoconducting antennas are capable of generating and coherently detecting subpicosecond electrical pulses. When illuminated these antennas with femtosecond optical pulses, radiate electrical pulses which have frequency spectra that extend from < 100GHz to > 2THz. Microscopic dipoles measuring 50, 100, and 200 μm have been fabricated and tested. Integrated photoconductors of radiation-damaged silicon-on-sapphire were used both for impulsive current excitation of the transmitting antennas as well as for gating the receiving antennas. Photoconductive antennas which are fabricated on ultrafast semiconductors, such as radiation-damaged silicon-on-sapphire (RD-SOS) or low-temperature grown GaAs (LT-GaAs) have been commonly used to detect subpicosecond electromagnetic pulses (THz) pulses. Photoconductive antennas based on semi-insulating (SI) GaAs with long carrier lifetime were shown by Sun et al [9] to be able to detect THz pulses. The detector, gated by femtosec laser pulses, produces output signals proportional to the integrated waveform of the incident THz pulses, in contrast to photoconductive detectors based on the high-speed semiconductors, whose output signals are proportional to the electric field amplitude of the incident THz pulses [10]. Masahiko Tani et.al [11] publication presented on the emission

characteristics of photoconductive antennas based on low-temperature-grown GaAs and semi-insulating GaAs. Several photoconductive antennas were fabricated on low-temperature GaAs and semi-insulating GaAs for terahertz generation. The radiation pattern of each photoconductive antenna was characterized with the photoconductive sampling techinique.The total radiation power was measured by bolometer for comparison of relative radiation power.

Naz E. Islam et.al [12] presented a publication on the various compensation mechanisms and response of high resistivity GaAs photoconductive switches for high-power applications. Semi-Insulating GaAs photoconductive switches are the switching component of high-power, ultra-wideband (UWB) microwave sources. In the GaAs, high resistivity can be achieved through various processing techniques. Liquid – encapsulated Czochralski (LEC) process with deep donor and shallow acceptor compensation mechanism highlight the characteristics of the PCSS such as breakdown voltage, rise time, and turn-on delay differences.

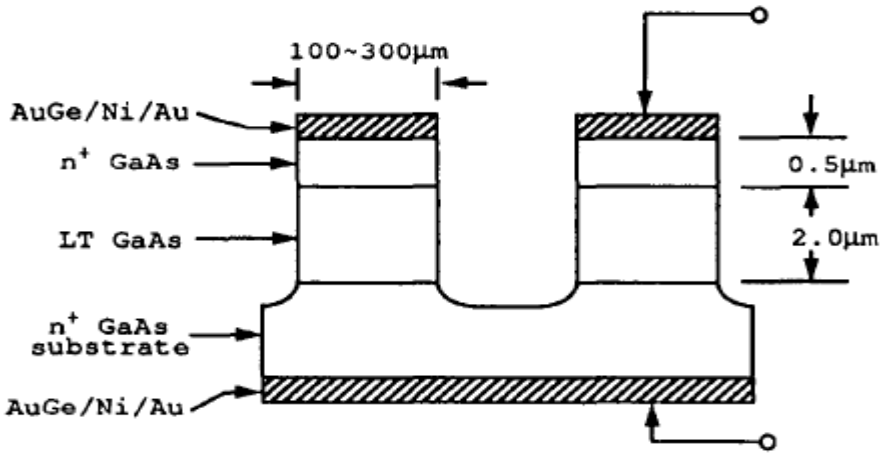

Figure 3. 1 Experimental test n-i-n structure Ref[13]

Bin Wu et.al [13] had devised an n-i-n structure at the University of California, Berkeley shown in Figure 3.1. The electrical properties of LT-GaAs were measured using n-i-n structure. The I-V characteristics showed three distinct regions. This model can be used in simulations of electrical device structures which incorporate LT-GaAs.

S. Gupta et.al [15] presented a publication on the epitaxially GaAs grown by molecular beam epitaxy at low-temperatures to study about subpicosecond carrier lifetime. By using femtosecond time-resolved-techniques, subpicosecond carrier lifetime is measured for GaAs grown by molecular beam epitaxy at ~200° C. Using the technique of electro-optic sampling measured the electrical pulses with a full-width at half-maximum of 0.6 ps. D. Liu et.al [17] presented that the temporal waveforms of THz pulses large-aperture antenna with its material of LT-GaAs have been studied. It was founded that the temporal waveforms have close relations with the specific carrier transport processes, especially since the carrier recombination for the semiconductor LT-GaAs of different growing temperatures plays a key role in the shaping of the bipolar structure of THz pulse.

J. Zhang et.al [19] developed a LT-GaAs photoconductive antenna for Terahertz pulse generation and detection is shown in Figure 3.2. It consists of a femtosecond laser, an optical delay line, an optical chopper, a THz emitter, a set of off-axis parabolodial mirrors for collimating and focusing the THz beam, a low- noise current preamplifier, and a lock-in amplifier. A CW diode-pumped, regenerative mode-locked Ti: sapphire

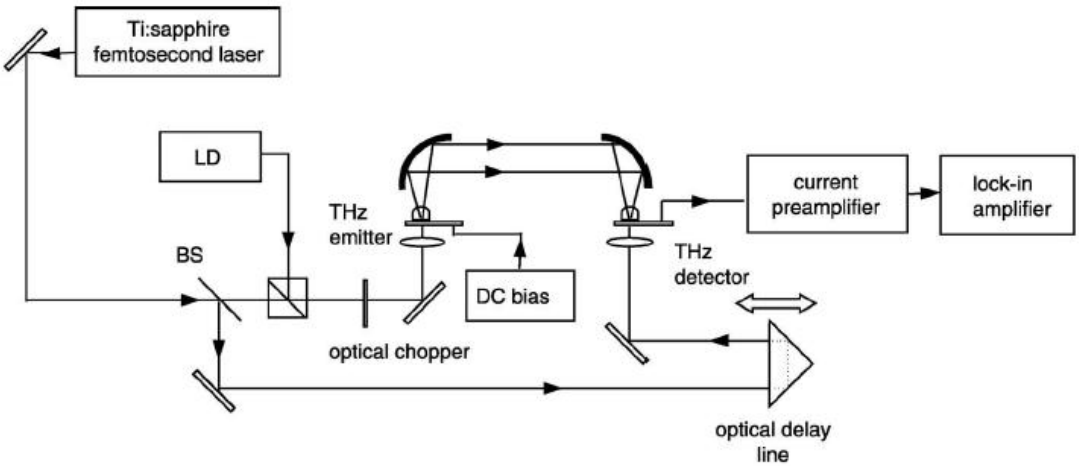

Figure 3. 2 Low-Temperature Gallium Arsenide photoconductive antenna for THz generation and detection Ref[19]

Laser (Mai Tai, Spectra-Physics), which gives a 100-fs pulse duration with >700 mW of average power and an 80 MHz repetition rate, was used to generate THz radiation.

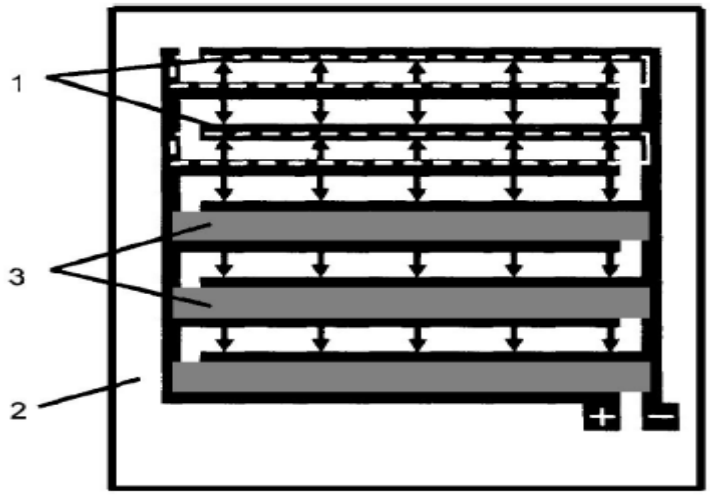

Figure 3. 3 Schematic sketch of the THz emitting MSM structure [23]

A. Dreyhaupt et.al [23] had look into the terahertz radiation from photoconductive MSM structures shown in Figure 3.3 to achieve unidirectional carrier acceleration on a

large area for high excitation powers. The emission is based on the intrinsic acceleration of carriers in PC and hence does not require a narrow-band antenna. High electric fields of the order of 100 kV/cm can be achieved by dc voltages of about 50V applied to the MSM structure, which eliminates the need for pulsed high power voltage supplies and this approach provides a broadband high-power THz emitter.

N. E. Islam et. Al [31] presented the liquid encapsulated Czochralski grown, highly resistive SI-GaAs PCSS for developing ultrawide band high power microwave radiation sources. Two sets of inputs models were used in the simulations. Model I is based on the current transport parameters such as concentration field mobility, auger recombination, impact ionization, SRH, etc. Model II includes model 1 features and in addition supports the formation of subsurface conduction channel either due to high field conditions or because of incomplete bonds and passivation layer interactions.

Phumin Kirawanich et.al [39] presented a field-carrier transport approach to analyze enhanced terahertz pulse power and frequency. PCSS excited through femtosecond lasers provides better spectral band-width and intensity. Biased PCSS antennas are fabricated by depositing two shaped electrodes on semiconductor wafers. The electrode configuration proposed will increase the emitted terahertz frequency spectrum for broadband applications and also enhance the peak power. N. E. Islam [45] presented a 3-D finite-difference time-domain analysis of a photoconductive-semiconductor-switch based terahertz (THz) source, integrated with a standard dipole and large-aperture radiator. LT-GaAs material was because of subpicosecond carrier lifetime, reasonably good carrier mobility, and relatively high breakdown field. The radiation from the PCSS large-aperture antenna is higher than that from the PCSS dipole antenna.

Y. C. Shen et.al [54] presented a biased and asymmetrically excited low-temperature grown GaAs photoconductive emitter, and characterized with a 20-μm-thick ZnTe crystal using free-space electro-optic sampling for terahertz radiation. The backwards THz radiation is collected in the measurement leading to the enahanced bandwidth.

CHAPTER 4: DEVICE SIMULATION

This chapter provides the device simulation of photoconductive semiconductor switches. The specific mathematical models and equations used in the design are also incorporated and discussed here.

4.1 Silvaco Software

Silvaco is a leading marketer among the electronic design automation (EDA) software and technology computer aided design (TCAD) process and device simulation software companies. Analog semiconductor process, device and design automation solutions in CMOS, bipolar, GaAs and compound technologies are provided by SILACO. User defined functions can be incorporated in the code through a C – interpreter. The physically – based simulation capabilities can be acquired using SILVACO. ATHENA, ATLAS, SmartSpice, Gateway, etc., are some of the major tools that are included in this software. The devices in this thesis were built using Devedit and the simulations were run in Silvaco TCAD Atlas software.

4.1.1 ATLAS

Atlas allows simulating the thermal, optical, and electrical behavior of semiconductor devices. It allows physics – based, easy to use, modular, and extensible platform to analyze AC, DC, and the time domain responses for all semiconductor based technologies in two dimensional and three dimensional. It provides insight into the

internal physical mechanisms associated with device operation. In SILVACO's VIRTUAL WAFER FAB simulation environment ATLAS is used as a core tool.

The information that flows in and out of ATLAS is shown in Figure 4.2. Atlas simulations use text file and structure file as input files. The input text file contains commands for ATLAS to execute. The other input file is a structure file that defines the structure that will be simulated. Runtime Output, Log Files, and Solution Files are the three types of outputs produced by ATLAS. The runtime output gives the progress and the error and warning messages as the simulation proceeds. The log file stores all terminal voltages and currents from the device analysis. The solution file stores two dimensional and three dimensional data relating to the values of solution variables within the device at a given device point.

ATLAS is used in conjunction with the DECKBUILD run-time environment, which supports both interactive and batch mode operation. An ATLAS command file is a list of commands for ATLAS to execute. In an ATLAS input file the order of statements is important. The five groups of statements must be in order in an ATLAS input file. Any change in the order of five groups will display an error message, which may result in incorrect operation or termination of the program.

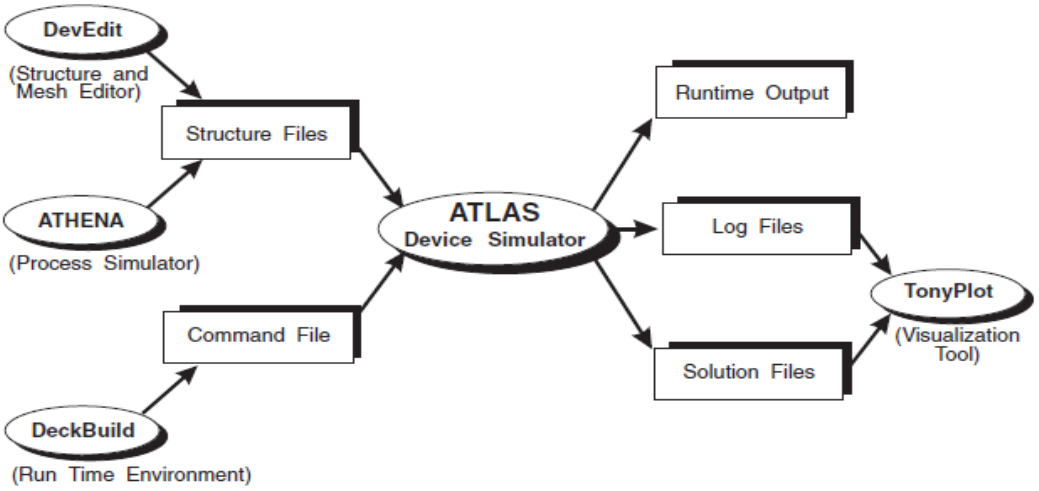

Figure 4. 1 Atlas Inputs and Outputs

Within the mesh definition, structural definition, and solution groups, the order of statements is also important. Otherwise, it will result in incorrect operation or termination of the program.

Group	*Statements*
1. Structure Specification	MESH REGION ELECTRODE DOPING
2. Material Models Specification	MATERIAL MODELS CONTACT INTERFACE
3. Numerical Method Selection	METHOD
4. Solution Specification	LOG SOLVE LOAD SAVE
5. Results Analysis	EXTRACT TONYPLOT

Figure 4. 2 ATLAS Command Groups with the Primary Statements in each group

The command groups with the primary statements in each group are shown in Figure 4.2. Devedit is used to create a new device or to remesh or edit an existing device. Using devedit, Silvaco structures can be easily integrated into Silvaco two dimensional and three dimensional simulators and other supporting tools. It consists of a region module that allows for the defining of an electrode location, name, and work function. It allows combining multiple 2D devices to create new 2D doping profiles. High quality triangle meshes can be created with minimal obtuse triangles. It also supports defining and meshing of 3D structures.

ATHENA simulator has developed from a world – renowned Stanford University simulator SUPREM – IV, with many new capabilities developed in collaboration with academic and industrial partners. It integrates many process simulation modules within a user – friendly environment provided by Silvaco TCAD tools. In semiconductor industry, it provides a compatible environment for simulating processes: ion implantation, diffusion, oxidation, physical etching and deposition, lithography, stress formation and silicidation. It provides fast and more accurate simulation of all critical fabrication steps used in CMOS, bipolar, SiGe/SiGeC, SiC, SOI, III – V, optoelectronics, MEMS, and power device technologies. Stresses in various device structures, dopant distributions, and multi - layer topology can be predicted accurately. It allows easy creation and modification of process flow input decks including automatic control of layout masks sequences, user – defined mesh generation and control, interactive plotting of 2D structures and distributions as well as 1D cross – sections, run-time excitation of important process and device parameters, and optimization of process flow and calibration of model parameters.

All Silvaco's TCAD and several other SIMUCAD products can run using DECKBUILD. It has powerful extract statements. It supports constructs such as loops and Boolean operations. It has many features such as kill, pause, stop at, and restart. It has the feature of invoking other tools from the tool box or directly from the input file. It supports numerical results from previous extract statements can be used as inputs to subsequent extract statements. It supports graphical user interface auto – creation of ATHENA process simulation input files. It allows automatic cyclical optimization of any parameter.

TONYPLOT is a powerful visualization tool to visualize the outputs produced by Silvaco TCAD simulators. It provides graphical features like pan, zoom, views, labels and multi plots. The data can be exported in many formats include; jpg, png, bmp, Spice Raw File and CSV. It allows overlay of many plots to compare their characteristics. It has tools which are integrated with ruler, probe, cutline, tracers, movie, HP-4145, movie. It supports contour data, vector data, meshed data, smith charts and polar charts, x-y data. It also supports linear scale, log scale and mixed scale. It allows creating meaningful labels to the plots. It allows one dimensional cutlines from two dimensional structures to study various characteristics of the device include; electric field, hole concentration, recombination rate, etc.

The visual and graphical images associated with the simulation tool gives information on device structures, recombination rate profile, current density profile, I – V characteristic profile, photogeneration rate profile, Donor concentration profile and other important profiles that might help in analyzing the device characteristics. The output data

is exported into excel data and easily be plotted. For any other information about the Silvaco software can be found in reference [33].

4.2 Nonlinear Equations

Three nonlinear equations must be solved to gain insight into the conduction mechanism of the photoconductive semiconductor switch devices.

--- Poisson's Equation

Poisson's Equation is defined by relating the electrostatic potential to the space charge density:

$$div(\varepsilon \nabla \psi) = -\rho \tag{4.1}$$

Where ε is local permittivity, ψ is electrostatic potential, ρ is local space charge density

--- Carrier Continuity Equations

The carrier continuity equations for electrons and holes are given by equations:

$$\frac{\partial n}{\partial t} = \frac{1}{q} div\vec{J}_n + G_n - R_n \tag{4.2}$$

$$\frac{\partial p}{\partial t} = \frac{1}{q} div\vec{J}_p + G_p - R_p \tag{4.3}$$

Where n and p are electron and hole concentrations respectively, $\vec{J}_n$ and $\vec{J}_p$ are electron and hole current densities respectively, G_n and G_p are generation rates for electrons and holes respectively, R_n and R_p are recombination rate for electrons and holes respectively, q is magnitude of the charge on an electron.

But additional secondary equations are required to specify particular physical models for current densities, recombination and generation rates.

4.3 Carrier Generation – Recombination Models

Carrier generation – recombination is the process through which the semiconductor material attempts to return to equilibrium after being disturbed under continual excitation. The following models are used in the device simulation:

--- Shockley-Read-Hall (SRH) Recombination

Phonon transitions occur in the presence of a trap (or defect) within the forbidden gap of the semiconductor. The Shockley-Read-Hall recombination is modeled as follows:

$$R_{SRH} = \frac{pn - n_{ie}^2}{TAUP0\left[n + n_{ie} \exp\left(\frac{ETRAP}{kT_L} \right) \right] + TAUN0\left[p + n_{ie} \exp\left(\frac{-ETRAP}{kT_L} \right) \right]} \tag{4.4}$$

Where ETRAP is difference between the trap energy level and the intrinsic Fermi level, T_L is lattice temperature in degrees Kelvin, $TAUN0$ and $TAUP0$ are electron and hole lifetimes respectively.

Since trap- assisted recombination occurs, Shockley-Read-Hall (SRH) recombination model was employed.

--- Auger Recombination

Auger recombination occurs through a three particle transition: an electron and a hole, which recombines in a band-to-band transition and gives off the resulting energy to

another electron or hole. Auger recombination is commonly modeled using the expression as follows:

$$R_{Auger} = AUGN(pn^2 - nn_{ie}^2) + AUGP(np^2 - pn_{ie}^2) \quad (4.5)$$

where the model parameters $AUGN$ and $AUGP$ are user-definable. The expression for the net recombination rate is similar to that of band-to-band recombination but includes the density of the electrons or holes, which receives the released energy from the electron-hole annihilation. Since recombination at high concentration of carriers involve, auger recombination model was employed.

4.4 Impact Ionization Models

In any space charge region with a sufficiently high reverse bias, the electric field will be high enough to accelerate free carriers up to the point where they will have acquired sufficient energy to generate more free carriers when in collision with the atoms of the crystal. In order to acquire sufficient energy, two principle conditions must be met. First, the electric field must be sufficiently high. Then, the distance between the collisions of the free carrier must be enough to allow acceleration to a sufficiently high velocity.

--- Selberherr's Impact Ionization Model

The ionization rate model proposed by Selberherr is a variation of the classical Chynoweth model. This model is activated by using the SELB parameter of the IMPACT statement, which is given by following expressions:

$$\alpha_n = AN \exp\left[-\left(\frac{BN}{E}\right)^{BETAN}\right] \quad (4.6)$$

$$\alpha_p = AP \exp\left[-\left(\frac{BP}{E} \right)^{BETAP} \right] \tag{4.7}$$

Where E is electric field in the direction of current flow at a particular position in the structure, AN and BN are function of the lattice temperature. To investigate the role of the impact ionization process on the device performance, Selberherr's model was employed.

4.5 Band-to-Band Tunneling

If a sufficiently high electric field exists within a device, local band bending may be sufficient to allow electrons to tunnel, by internal field emission, from the valence band into the conduction band. An additional electron is therefore generated in the conduction band and a hole in the valence band. This generation mechanism is implemented into right-hand side of the continuity equations. The tunneling generation rate is [100,101,102,121] as:

$$G_{BBT} = BB.A \;\; E^{BB.GAMMA} \exp\left(-\frac{BB.B}{E} \right) \tag{4.8}$$

Where E = magnitude of an electric field and BB.A, BB.B and BB.GAMMA are user definable.

The model parameters set to the standard model [100] by specifying BBT.STD on the MODELS statement. The parameter default values:

BB.A = 9.6615e18 $cm^{-1}V^{-2}s^{-1}$ BB.B = 3.0e7 V/cm BB.GAMMA = 2.0

Since GaAs is a direct band gap material, band to band tunneling model was employed.

4.6 Non-Linear Iteration

The non-linear solution method, and associated parameters such as iteration and convergence criteria, is specified in the METHOD statement. Non-linear iteration solution methods are specified in the METHOD statement using the NEWTON, GUMMEL, or BLOCK parameters.

--- Newton Iteration

Each iteration of the Newton method solves a linearized version of the entire non-linear algebraic system. The size of the problem is relatively large, and each iteration takes a relatively long time. The iteration, however, will normally converge quickly as long as the initial guess is sufficiently close to the final solution. To reduce the possibility of divergence problem, newton iteration was employed.

4.7 Traps and Defects in Semiconductors

Semiconductor materials exhibit crystal flaws, which can be caused by dangling bonds at interfaces or by the presence of impurities in the substrate. The presence of these defect centers, or traps, in semiconductor substrates may significantly influence the electrical characteristics of the device. Trap centers, whose associated energy lies in a forbidden gap, exchange charge with the conduction and valence bands through the emission and capture of electrons. The trap centers influence the density of space charge in semiconductor bulk and the recombination statistics.

A donor – type trap can be either positive or neutral like a donor dopant. An acceptor-type trap can be either negative or neutral like an acceptor dopant. A donor-like

trap is positively charged (ionized) when empty, and neutral when filled (with an electron). An empty donor-type trap, which is positive, can capture an electron or emit a hole. A filled donor-type trap, which is neutral, can emit an electron or capture a hole. An acceptor like trap is neutral when empty and negatively charged (ionized) when filled (with an electron). A filled acceptor-like trap can emit an electron or capture a hole. An empty acceptor-like trap can capture an electron or emit a hole. Unlike donors, donor-like traps usually lie near the valence band. Likewise, acceptor-like traps usually lie near the conduction band. Figure 4.3 shows to define the type of trap.

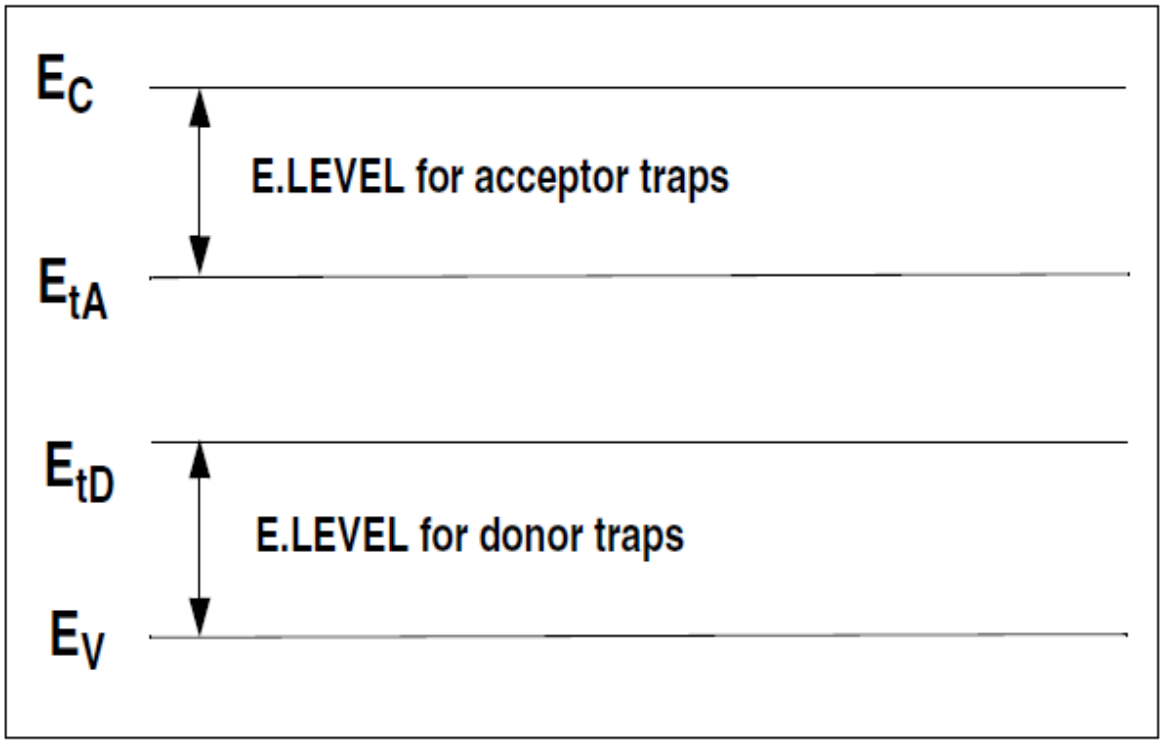

Figure 4. 3 Definition of the trap energy level for acceptor and donor traps in reference to the conduction and valance band edges

The position of the trap is defined relative to the conduction or valence bands using E.LEVEL.

For any other information about the models can be found in reference [33].

4.8 Parameters used in the simulation

- Carbon is used as acceptor with density 2.5e15 /cm^3 for Low – Temperature Gallium Arsenide
- Carbon is used as acceptor with density 3e15 /cm^3 for Semi - Insulating Gallium Arsenide
- Trap concentration is 3.006e15 /cm^3
- Lateral Aluminum contacts
- Energy level is 0.732eV from valence band
- Electron capture cross – sections : 3e-10
- Hole capture cross – sections : 1e-10
- Recombination models are Auger and SRH
- Mobility models are fldmob (field dependent mobility) and conmob (concentration dependent mobility)
- Impact Ionization model is Selberherr's model
- Band-to-Band Tunneling
- Monochromatic Beam with photon density of 0.5 W/μm^2 with wavelength of 780nm at an angle of 90 degrees

4.9 Mesh Simulation

In the process simulation, the correct specification of mesh is very critical. A finer mesh must be contained in the areas where the p – n junction will be formed; optical illumination may change photoactive component concentration, and ion implantation will occur. The total number of nodes in the grid N_p has a direct effect on simulation time and accuracy. Using the finite element analysis method, the total number of arithmetic operations that are necessary to achieve a solution for processes simulated can be estimated as $(N_p)^{\alpha}$. In order to maintain the simulation time within the reasonable bounds, the finer grid would not be allowed to shed into unnecessary regions of the device.

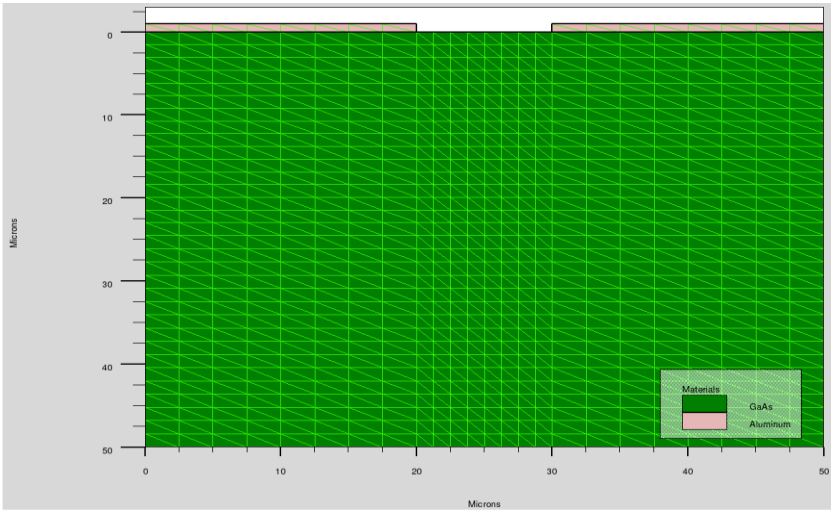

Figure 4. 4 Simulation Mesh

The Figure 4.4 shows the simulation mesh for the device designed in the research. To avoid the convergence problem the mesh is refined finer in both X and Y direction. The important parameter in obtaining correct simulation results is the mesh. The typical areas are trap filling areas, high impact ionization areas, and high electric fields near the electrodes. The crucial factors to consider are avoiding obtuse triangles in

the current path, avoiding abrupt discontinuities in the mesh, and making sure that high field areas have high mesh density.

CHAPTER 5: RESULTS AND DISCUSSION

This chapter discusses the simulation results for the substrate conditions and other carrier characteristics in LT GaAs and SI-GaAs PCSS during Terahertz (THz) generation. As mentioned earlier, all the simulations were executed using Silvaco TCAD Atlas software.

5.1 PCSS Devices Studied

In this research work, two different photoconductive semiconductor switches for Terahertz pulse generation are studied. One was the Semi-Insulating Gallium Arsenide PCSS, and the other was Low-Temperature Gallium Arsenide PCSS.

5.1.1 Semi-Insulating Gallium Arsenide (SI-GaAs) PCSS

Figure 5.1 shows the simulation mesh of Semi-Insulating Gallium Arsenide PCSS which has contacts on the lateral side of the wafer. The active region (distance between the contacts) is 10 μm, and the contacts are made from layered Aluminum of thickness 1.3 μm. The length and the width of the device are 50 μm X 50 μm. The material used in this photoconductive semiconductor switch is Liquid-Encapsulated Czochralski (LEC) grown GaAs, in which deep donors are compensated by shallow acceptors (DDSA). In the DDSA compensation scheme, a balance is obtained between the EL2 and shallow acceptor impurity which is generally carbon. The bulk resistivity is in the order of 10^7-10^8 Ω-cm. SI-GaAs exhibits crystal flaws, due to the presence of dangling bonds at interfaces or due to the presence of impurities in the substrate [49]. The presence of these

traps or defect centers in the material may significantly influence the electrical characteristic of the devise [50]. Trap centers exchange charge with the valence and conduction band through the emission of electrons and recombination. The trap centers change the density of the space charge and hence influence recombination characteristics [51, 52].

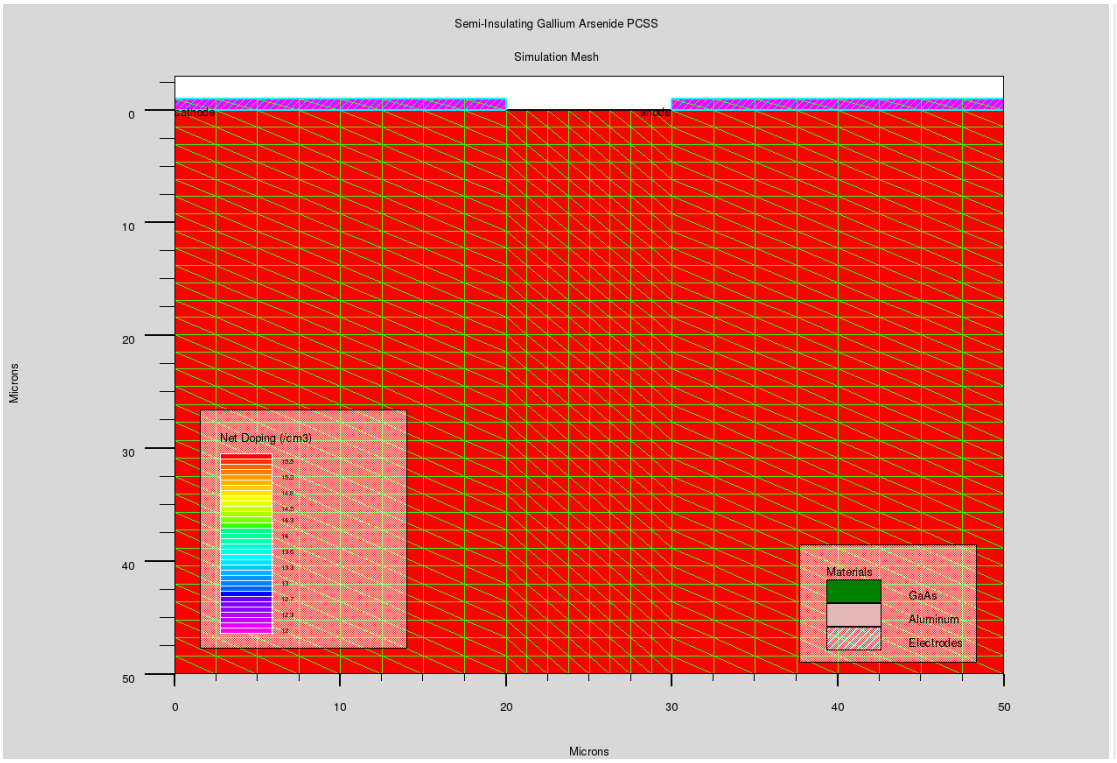

Figure 5. 1 Semi-Insulating Gallium Arsenide (SI-GaAs) PCSS

The optically activated switches discussed here is a bulk Semi-Insulating (SI) GaAs semiconductor. The material that is in intimate contact with the device is Al. The compensation mechanisms discussed earlier for the semi-insulating semiconductor material is implemented as follows. The material is a deep donor and a shallow acceptor

type compensated semi-insulating semiconductor. Hence a 3 X 10^{15} atoms/cc carbon doping represents the shallow accepter dopanted which is compensated by a deep donor of EL2 at 0.732 eV trap level. The trap concentration is 3.006 X 10^{15} /cm^3. Details on the compensation scheme can be found in reference [31].

5.1.2 Low-Temperature Gallium Arsenide (LT-GaAs) PCSS

The Figure 5.2 shows the cross section of Low-Temperature Gallium Arsenide PCSS which has contacts on the lateral side of the wafer. The structure is similar to SI-GaAs PCSS where the distance between the contacts is 10 μm and the contacts are made from layered Aluminum of thickness 1.3 μm. The dimension of the device is 50 μm X 50 μm. The material used in this photoconductive semiconductor switch is Low-Temperature grown GaAs (LT-GaAs), which is GaAs grown at a temperature of 200 – 300^0, usually with a slight excess of Arsenic. The GaAs is grown at low temperatures, the sticking coefficient of As is increased and more Arsenic is incorporated at the growth interface. This leads to an excess As- percentage of 1-2%, which was determined by Auger Electron Spectroscopy (AES) and Secondary Ion Mass Spectroscopy (SIMS) [55] and it results in a highly non-stoichiometric material with a lattice constant of about 0.1 % [56] larger than normal molecular beam epitaxy (MBE) grown GaAs as revealed by the X-ray rocking curves . LT-GaAs has subpicosecond carrier lifetime, reasonably good carrier mobility, and relatively high breakdown field [45].

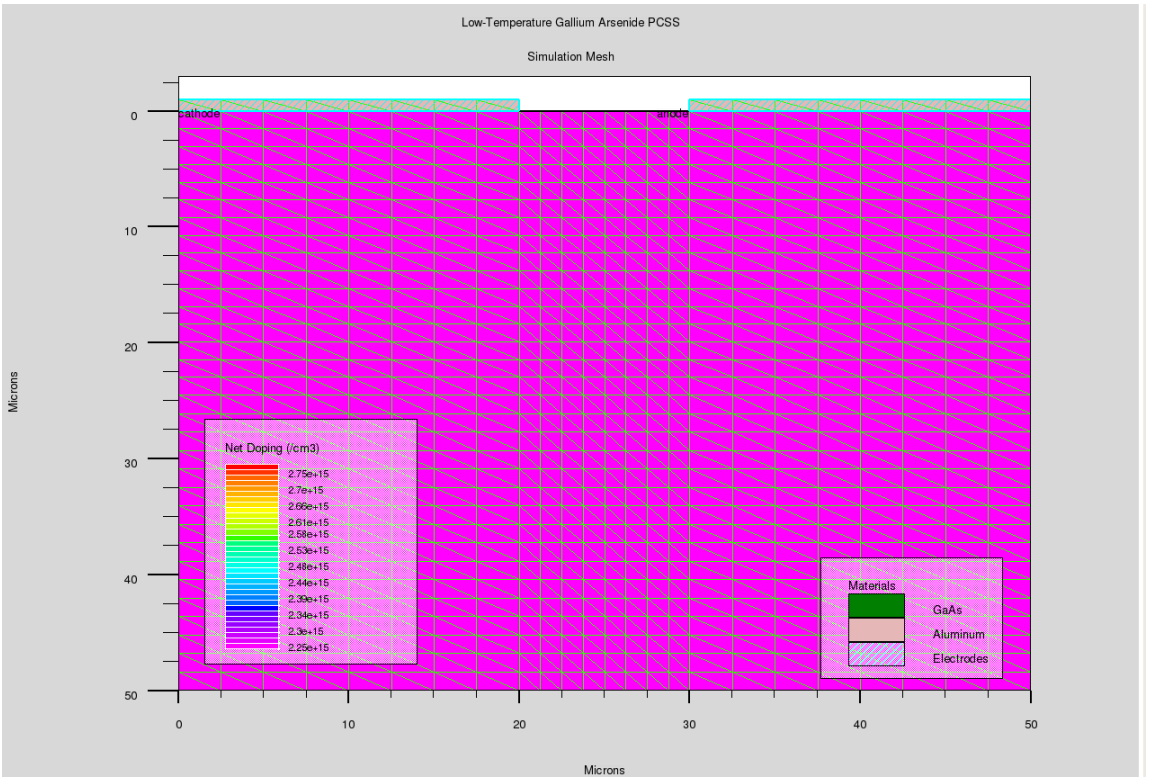

Figure 5. 2 Low-Temperature Gallium Arsenide (LT-GaAs) PCSS

The optically activated switches discussed here are a semiconductor device which consists of Low-Temperature Gallium Arsenide. The material that is in intimate contact with the device (Al) has been used and it is not expected to effect the results since the contact material will dominate conduction. The method is discussed earlier for the low-temperature semiconductor material is implemented as follows. The material which is GaAs grown at a temperature of 200 – 300^0, usually with a slight excess of Arsenic. A 2.5 X 10^{15} /cm^3 carbon doping and a 0.732 eV EL2 trap level used. The trap concentration is 3.006 X 10^{15} /cm^3. More information can be found in reference [13].

5.2 Simulation Results and Discussion

Simulations were done in two stages. First the structures were charged to high bias state in steps and then the high bias structures were then illuminated with optical pulses and the response of the PCSS noted. The initial bias voltages were set from 5V to 250V in steps. The LT-GaAs PCSS and SI-GaAs PCSS were excited by optical pulses with a pulse width of 80 fs (FWHM), a photon density of 0.5 $W/\mu m^2$, and a wavelength of 780 nm.

5.2.1 Analysis of I-V Characteristics

The Figure 5.3 shows the simulated I-V characteristics of LT-GaAs PCSS and SI-GaAs PCSS. From the I-V characteristics, the behavior of the devices can be explained. The I-V characteristic of the SI-GaAs PCSS with EL2 traps as determined through simulation is very similar to the one explained by Lampert and Mark for a trap-filled material [53]. According to Lampert and Mark theory, the voltage decreases with increasing current through the negative resistance region to a minimum, V_m, after it starts to rise again. The current increase, following $V_{m,}$ must follow a V^2 dependence and then V^3 dependence. The current in the V^2 region is largely recombination limited and in V^3 region both recombination and space-charge limited. The I-V characteristic of the LT-GaAs is very similar to the one shown by Bin Wu [13]. As seen in Figure 5.3, the I-V curve is divided into three regions for both the PCSS. In region I, the current varies linearly with applied bias voltage which corresponds to linear domain. In region II, Fermi level has moved closer to the trap level which corresponds to trap-filled limited current domain. In the region III, Fermi level moved above the trap-filled level. The linearity of

I-V is more prominent in LT-GaAs than that of the SI- GaAs. The LT-GaAs also shows the higher resistivity when compared to SI-GaAs.

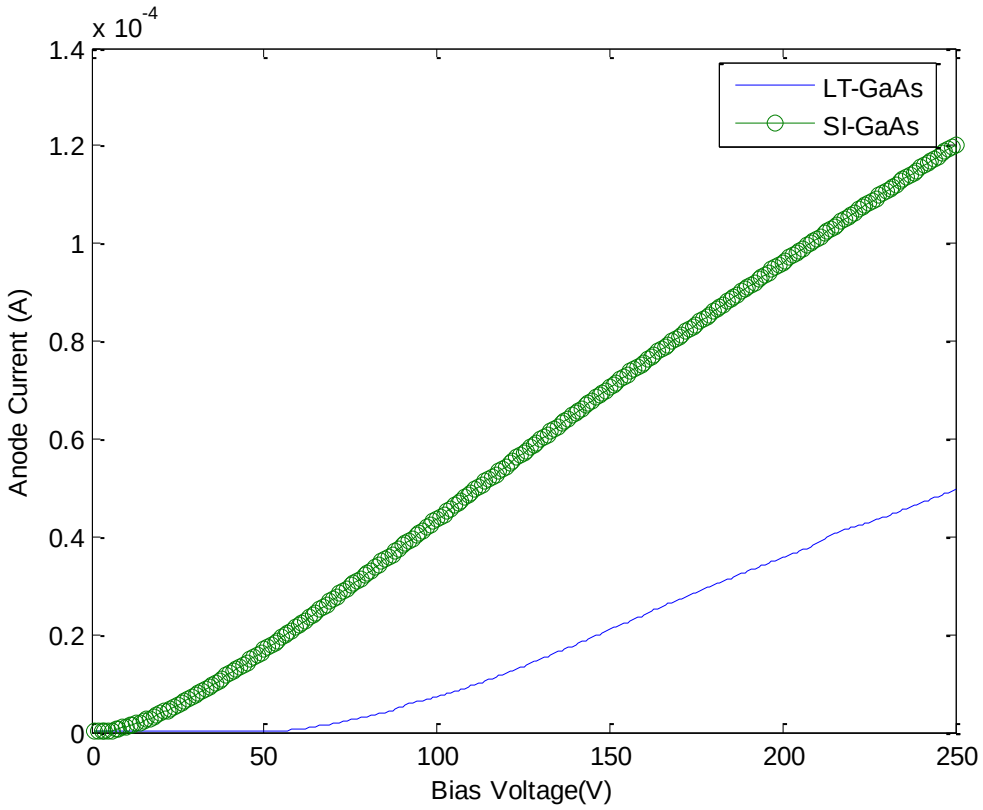

Figure 5. 3 I-V Characteristics of LT-GaAs PCSS and SI-GaAs PCSS

5.2.2 Analysis of Recombination Rate

Figures 5.4 and Figure 5.5 show profiles of the recombination rate of electron-holes for LT-GaAs PCSS and SI-GaAs PCSS, following the generation of carriers due to the laser pulse at 120 V and 250 V respectively. Recombination centers have relatively large capture cross sections for both types of carriers. Thus, trapping both the electrons and holes causing their devastation. The presence of several defect levels would cause the electrons and holes to be efficiently trapped at different levels. In this phenomenon the recombination would be limited by the re-emission of the trapped carriers back to their

respective bands. The mid gap EL2- like effect is the main recombination center in both the devices. It is noticed from the Figure 5.4 and 5.5 that the recombination rate is maximum in the devices at 25 μm length. This is due to the fact that concentration of electrons and holes is largest at that point. It has also been observed that there is an increase in recombination rate amplitudes with application of higher bias voltages. In contrast to the LT-GaAs, the recombination rate is higher in SI-GaAs. This is due to the relatively large trap concentration at mid gap in SI-GaAs.

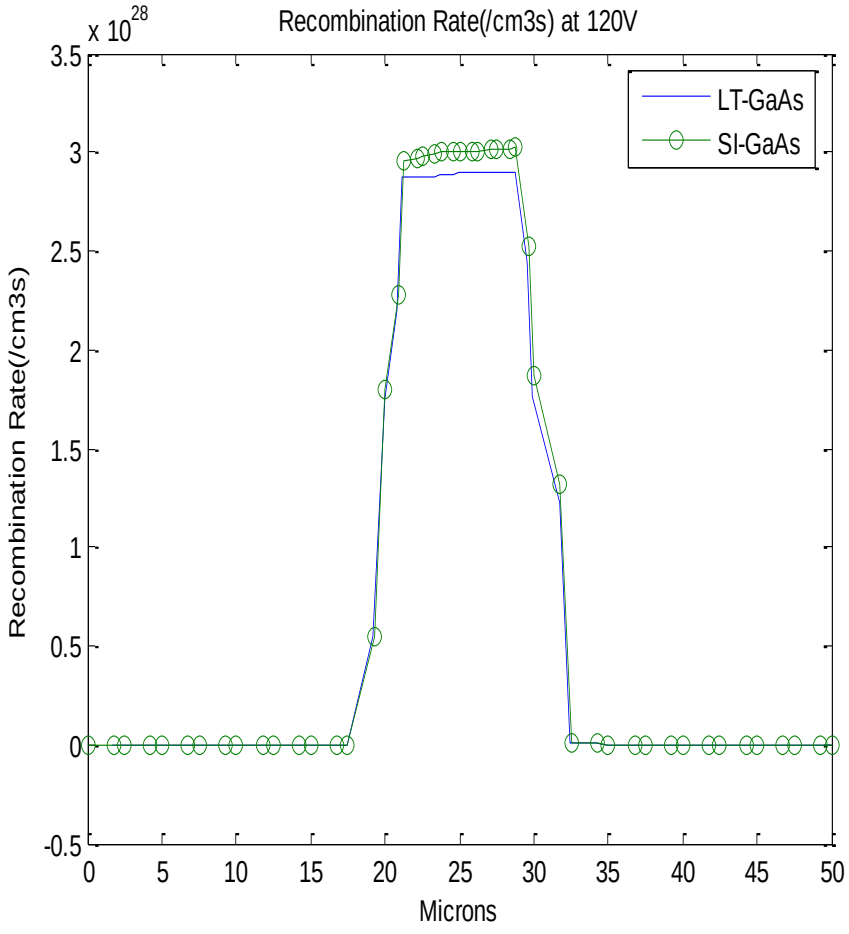

Figure 5. 4 Recombination Rate Profile of both PCSS at 120V

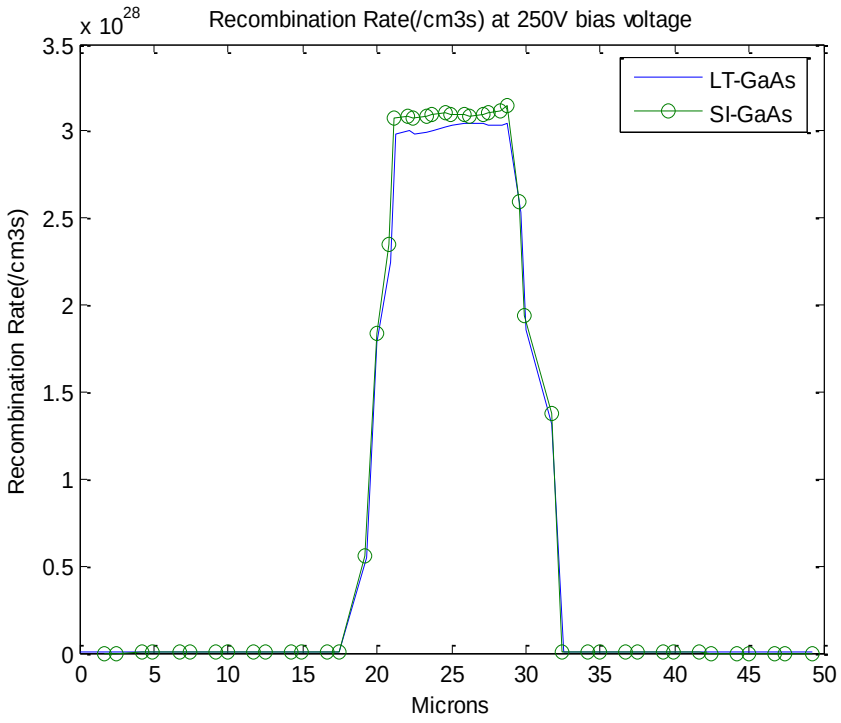

Figure 5. 5 Recombination Rate Profile of both PCSS at 250V

Figure 5.6 shows the overlay of the recombination rate contour profile with time before (t=0 fs), immediately at the end of laser pulse (t=80 fs) of both SI-GaAs and LT-GaAs PCSS respectively at 250V bias voltage. In Figure 5.6, the recombination rate in SI- GaAs around the depth of 25 µm is drastically decreased and in the depth of 30 µm it nearly approaches zeros. In Figure 5.8, the recombination rate in LT-GaAs around the depth of 22.5 µm is drastically decreased and in the depth of 27.5 µm it nearly approaches zero. It is observed that even though the recombination rate is higher in SI-GaAs compared to LT-GaAs, the collection depth much here for the SI-GaAs. As a result the total collected charge for the SI-based PCSS is much more than that of LT GaAs, as

will be shown later. Also because of lower recombination in LT GaAs, the rise time is much faster in this PCSS.

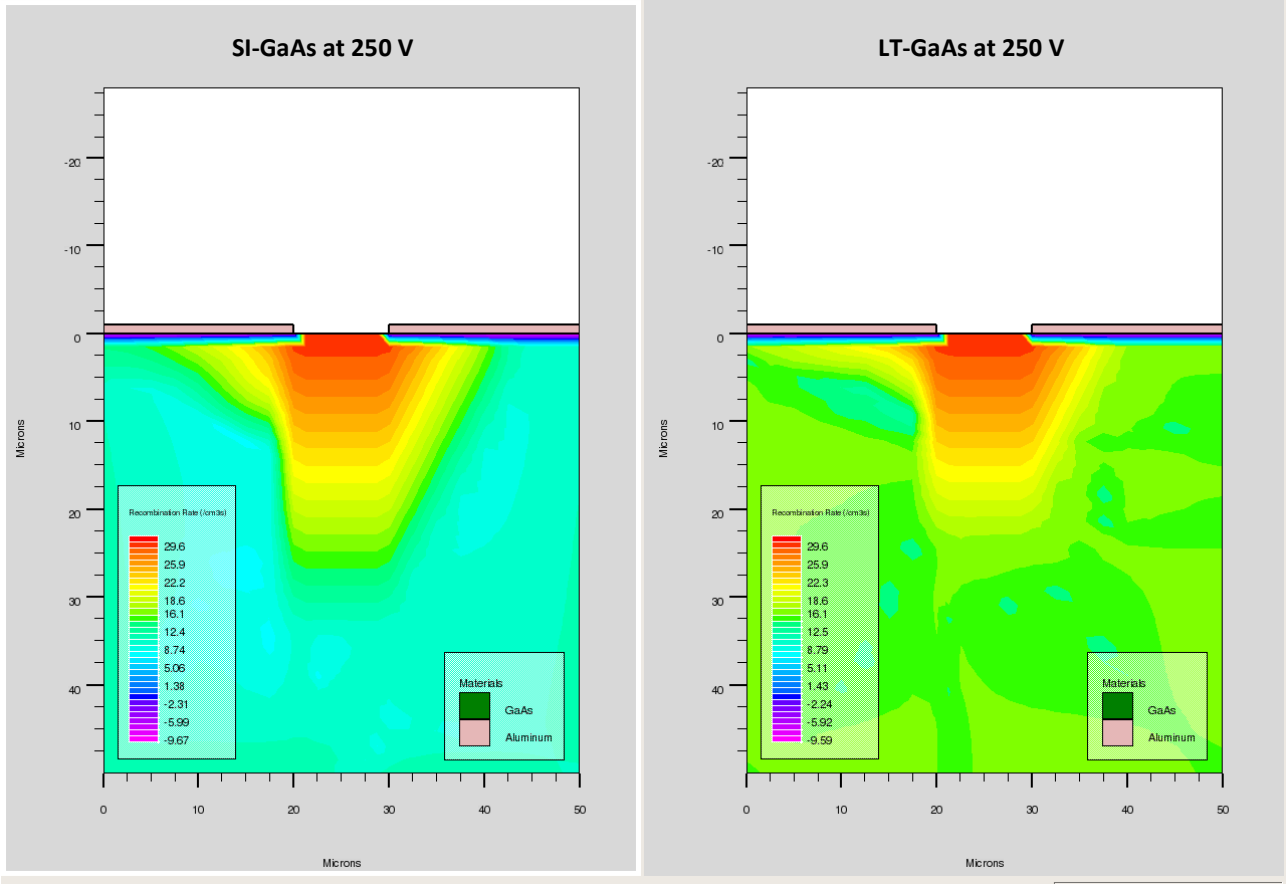

Figure 5. 6 Overlay of Recombination Rate contour profile with time before (t=0 fs), immediately at the end of laser pulse (t=80 fs) of both SI-GaAs and LT-GaAs PCSS respectively at 250V

5.2.3 Analysis of Total Current Density

The current density amplitude is a function the Electric field distribution at a given bias voltage. Due to the presence of high electric field intensities in the vicinity of each electrode, the current density also peaks in these regions. The mechanism of the

induced currents is described as follows. The nonuniform photo excitation induces transient electric field to redistribute inside the gap. This electric field redistribution cause the carrier concentration transient, where its time derivative is proportional to the current [45]. A decrease of current value before the carriers can recombine is due to the collapse of the total electrical fields as discussed by M. Tani et.al [10]. Figures 5.7 and Figure 5.8 show the current density profiles of LT-GaAs and SI-GaAs at 120V and 250V bias voltages respectively. It shows that there is an increase in current density amplitudes in both PCSS next to the electrodes with the application of bias voltages due to the increase in electric field, as discussed earlier. The peak of the SI-GaAs PCSS current density next to the anode is higher in comparison to the peak of LT-GaAs PCSS current density under same bias voltage because the electric field intensity is also higher at this region. Since the mobility of LT-GaAs is more compared to SI-GaAs, it means more electrons get collected at the anode for LT-GaAs as compared to SI-GaAs. Thus there is a crowding of charge near the anode for LT-GaAs PCSS which shields the electric field, making it lower than SI-GaAs.

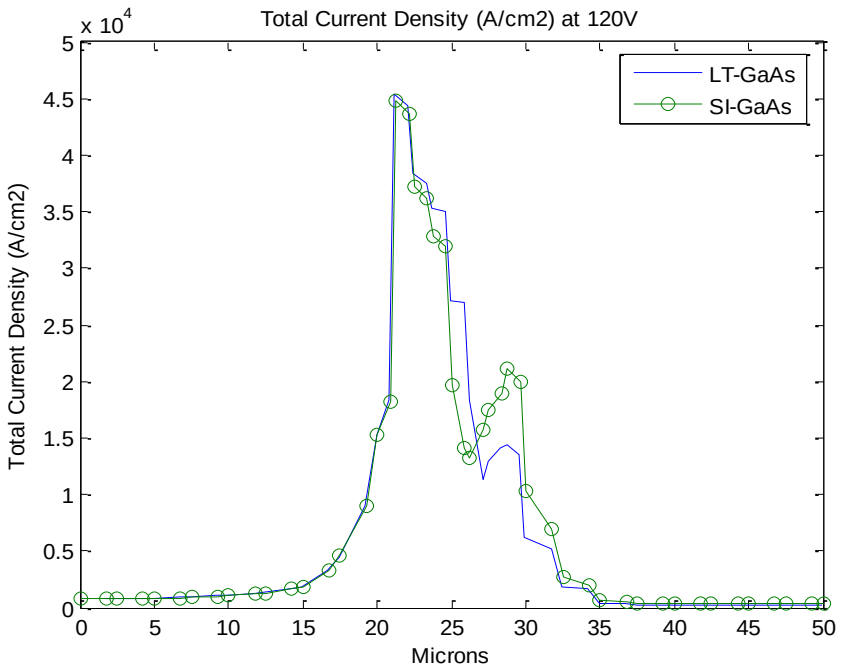

Figure 5. 7 Total Current Density Profile of both PCSS at 120V

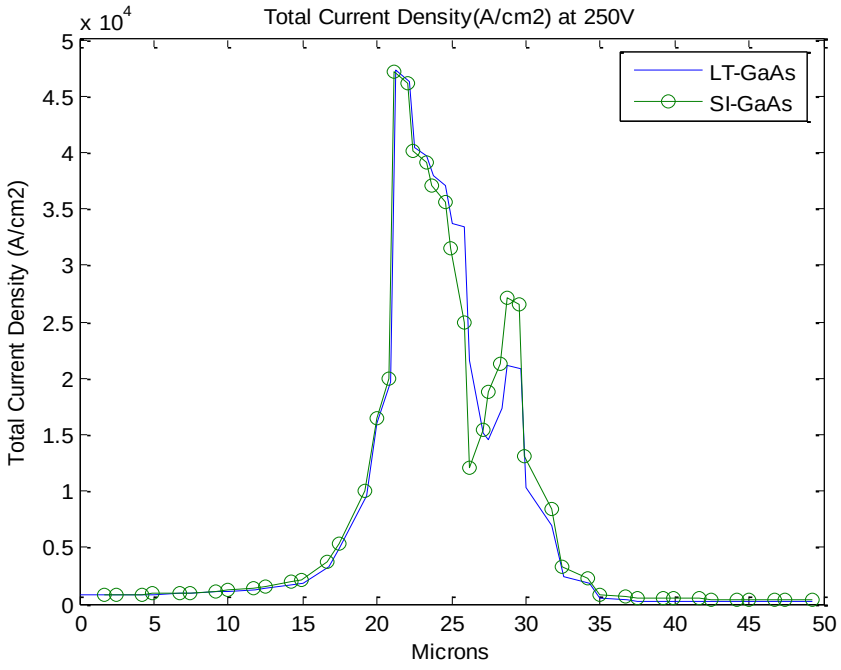

Figure 5. 8 Total Current Density Profile of both PCSS at 250V

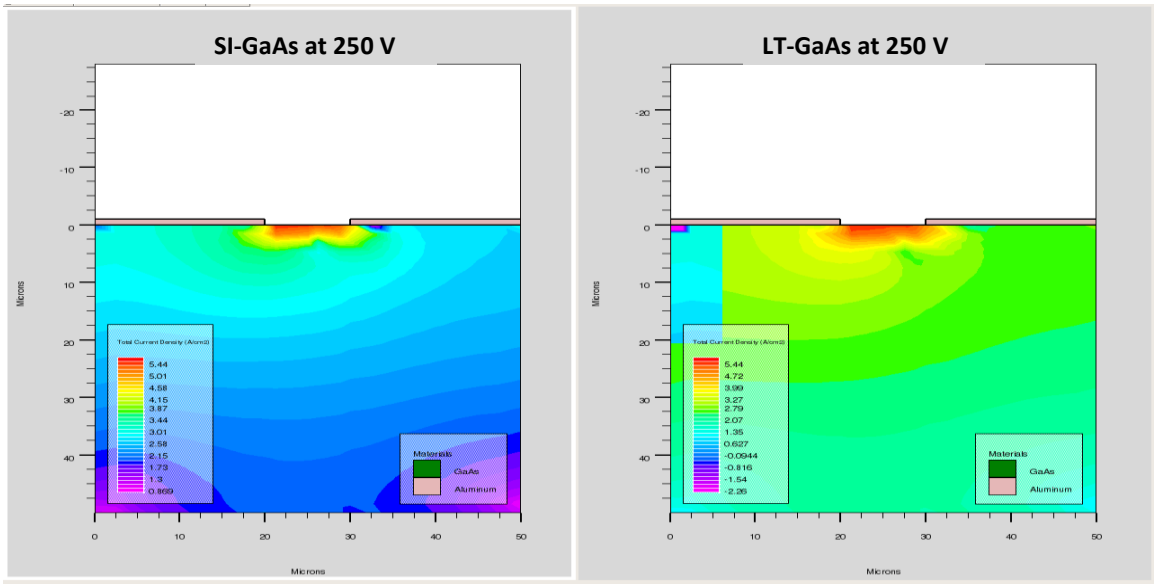

Figure 5. 9 Total Current Density contour profile with time before (t=0 fs), immediately at the end of laser pulse (t=80 fs) of both SI-GaAs, and LT-GaAs PCSS respectively

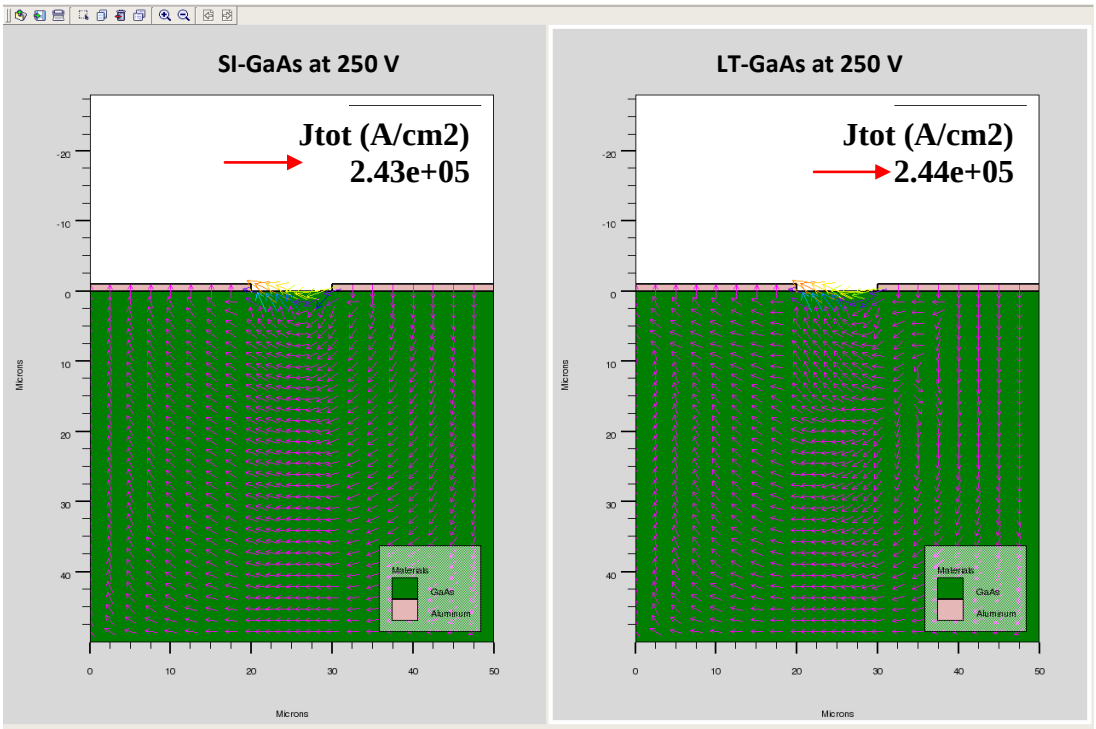

Figure 5. 10 Total Current Density vector profile with time before (t=0 fs), immediately at the end of laser pulse (t=80 fs) of both SI-GaAs, and LT-GaAs PCSS respectively

The Figure 5.9 shows the overlay of total current density contour profile with time before (t=0 fs), immediately at the end of laser pulse (t=80 fs) for both SI-GaAs and LT-GaAs PCSS respectively at 250V bias voltage. The Figure 5.10 shows the total current density vector profile with time before (t=0 fs), immediately at the end of laser pulse (t=80 fs) for both SI-GaAs and LT-GaAs PCSS respectively at 250V bias voltage. It can be seen that the total current density contour in both the PCSS shown in Figure 5.9, are not symmetric. Also the current vectors (Figure. 5.10), have an upward and left direction towards the cathode for both the PCSSs. This behavior is can be explained using Figure 5.7. Since the recombination rate and the mobilities of the carriers are different in the devices there will be difference in the rate at which these carriers are collected these devices are different. This produces an asymmetry in the charge collection as shown by the current density contour and its vectors profiles in Figures 5.9 and 5.10 respectively.

5.2.4 Analysis of On State Response

The Figure 5.11 shows the simulated on state response of the LT-GaAs PCSS and SI-GaAs PCSS at 120V and 250V bias voltages respectively. The LT-GaAs PCSS and SI-GaAs PCSS were excited by an optical pulse with a pulse width of 80fs (FWHM) which is incident on the active region with a power of $0.5W/\mu m^2$ having wavelength of 780nm [40]. When the active region is illuminated with the laser pulse a large number of optical-generated carriers are generated rapidly during the laser pulse duration. As a result the generated the current densities also increase rapidly due to the biased electric fields. Since the pulse width duration is less than the carrier lifetime, most the generated

carriers and the process of negative and positive peaks in THz emission follow, as discussed by Phumin Kirawanich [45] and briefly explained in the next paragraph.

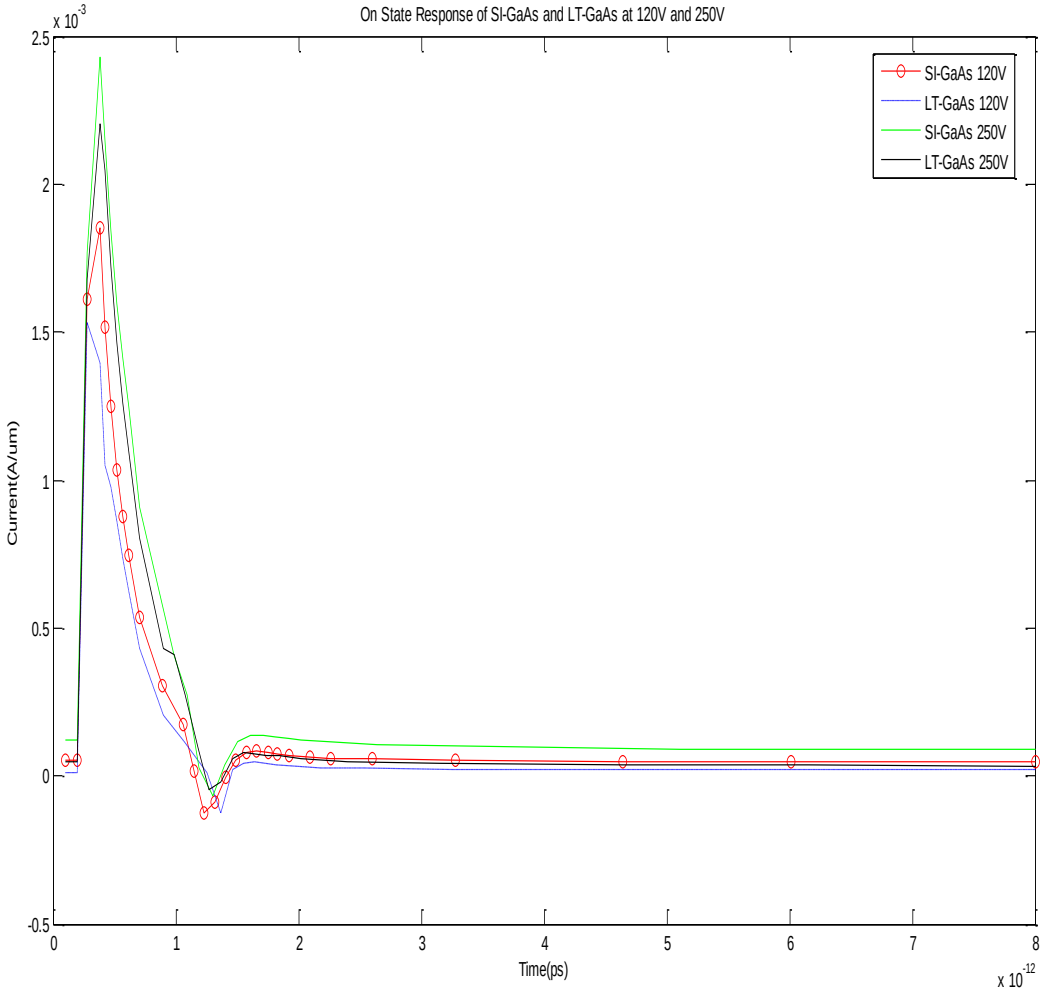

Figure 5. 11 On State Response of SI-GaAs PCSS and LT-GaAs PCSS at 120V and 250V respectively

The positive peak is attributed to the strong onset of the photocurrent which is influenced by the acceleration of carrier generation under bias field, while the negative

peak primarily due the photocurrent that is decreasing due to the carrier recombination rate which is a function of the carrier lifetime. The rise of the THz pulseform is due to the electrons increase continuously in velocity and quantity during the period of electrons acceleration. The fall of the THz pulseform is due to the rate of increase in electrons quantity reduces, thus the change rate of current density decrease. As the velocity and the carrier concentration become constant, the THz pulse ceases to exist. The rise time in LT-GaAs PCSS is faster when compared to the rise time in SI-GaAs PCSS under same bias voltage. This can be attributed to the faster charge collection in LT-GaAs PCSS relatively to the SI-GaAs PCSS. A fast rise time also signals more energy transfer to the load [35].

CHAPTER 6: CONCLUSION

This chapter provides a summary of the research findings in the design of the PCSS, specifically as it relates to the substrate conditions and characteristics of LT- GaAs SI-GaAs PCSS during Terahertz pulse generation. Suggestions for future research in this area of work are also provided.

6.1 Summary of Work

Low-Temperature gallium Arsenide and Semi-Insulating Gallium Arsenide has been used as substrate materials for Terahertz (THz) pulse generation. An industry standard simulation suite, Silvaco, has been used in the analysis. Simulations were performed on LT–GaAs and SI–GaAs photoconductive semiconductor switches. Substrate properties of the two PCSS materials and their charge collection mechanism were studied. Specifically, the role of traps in the semiconductor materials, the effects of the trap density, concentration and capture cross section on collection rate that influences THz generation was examined. The effects of carrier rise time on beam width and decay was reviewed.

The following conclusions can be derived from the analysis:

- Conversion of time domain pulse to frequency domain show that both SI and LT grown GaAs PCSS can generate THz radiation.
- The conduction process (as seen in the I – V characteristic) in LT – GaAs is delayed as compared to the SI – GaAs is due to the trapping – detrapping of the electrons.

- As a result of relatively large trap concentration at mid gap in SI-GaAs, the carrier recombination rate profile is higher in SI–GaAs than in LT–GaAs.
- The total current density profile at the cathode is higher in LT–GaAs PCSS when compared to SI-GaAs PCSS. This is because at higher mobility in LT-GaAs is more compared to SI-GaAs at the same E-field (bias).
- The total current density profile at the anode is higher in SI–GaAs PCSS when compared to LT-GaAs PCSS. This is because of higher mobility in LT-GaAs the carriers reach the anode much faster and results in accumulation. Carrier collection is reduced as a result.

- For the same bias voltage, the total photo generated charge collected (area under the on state response plot) is more in SI–GaAs as compared to LT – GaAs. This is due to higher recombination is LT GaAs which results in a loss of charge.

In summary, the substrate properties of PCSS materials affect the characteristics of THz wave. The both LT-GaAs PCSS and SI-GaAs PCSS, the role of traps is an important factor that determines the generated pulse shape and width. Specifically effects of recombination rate, beam width and decay and carrier rise time influences the current density and the shape of THz pulse generated. Further, it was observed that LT-GaAs based photoconductive semiconductor switches have superior resistivity (breakdown fields) and charge collection values when compared to SI-GaAs based photoconductive semiconductor switches.

Future Work

Three specific research directions are proposed to further this study. First, although the current work substantially reduces the dimensions of the switch when compared to the current state-of-art, future work should focus on further reducing the size of the switches, thereby making switches more economically viable. Secondly the role of contact geometry and the separation distance between the contacts in THz generation should be studied. Finally, a study to optimize the applied bias voltage for THz pulse generation with maximum power needs to be conducted.

REFERENCES

[1] G. Mourou and W. Knox, Appl. Phys. Lett., vol. 35, p.492, 1979

[2] K. H. Schoenbach, V.K. Lakdawala, R. Germer and S.T. Ko, J. Appl. Phys., vol. 63, p. 2460, 1988.

[3] Stoudt D. C., Zutavern, Loubriel, "Subnanosecond High-Power performance of a bistable optically controlled GaAs switch"

[4] K.Horio, T.Ikoma, and H. Yanai, IEEE Trans. Electron Devices, 33(9), 1242-1250 (1986)

[5] Terahertz generation at jlab. Available : www.jlab.org

[6] G. Mourou, C. V. Stancampiano. A. Antonetti, and A. Orszag, "Picosecond microwave pulses generated with a subpicosecond laser driven semiconductor switch," *Appl. Phys. Lett.*, vol. 39, pp. 295-296, Aug. 15, 1981.

[7] D. Auston and M. Nuss, "Electrooptic generation and detection of femtosecond electrical transients," *IEEE J. Quant. Elec.*, vol. 24, no. 2, pp. 184-197, Feb. 1988.

[8] P. Smith, D. Auston, and M. Nuss, "Subpicosecond photoconducting dipole antennas," *IEEE J. Quant. Elec.*, vol. 24, no. 2, pp. 255-260,1988

[9] F. G. Sun, G. A. Wagoner and X.-C. Zhang: Appl. Phys. Lett. 67 (1995) 1656

[10] M. Tani, K. Sakai and H. Mimura, "Ultrafast photoconductive detectors based on semi-insulating GaAs and InP," *Jpn. J. Appl. Phys.*, vol. 36, pp. L1175-L1178, Sep. 1997.

[11] M. Tani, S. Matsuura, K. Sakai, and S. Nakashima, "Emission characteristics of photoconductive antennas based on low-temperature-grown GaAs and semi-insulating GaAs," *Appl. Opt.*, vol. 36, no. 30, pp. 7853-7859, Oct. 1997.

[12] Islam N.E, Schamiloglu E, Schoenberg J. S. H, Joshi R.P.;" Compensation Mechanisms and the Response of High Resistivity GaAs Photoconductive Switches During High-Power Applications", IEEE Trans. On Plasma Science, VOL 28, No 5, October 2000.

[13] Bin Wu, Ashish Verma, John Gamelin, Hyunchul Sohn*, Shyh Wang "Characterization of Electrical Properties of Low Temperature GaAs", Mat. Res. Soc. Symp. Proc. Vol. 241 , 1992 Materials Research Society

[14] X.-C. Zhang, J. T. Darrow, B. B. Hu, D. H. Auston, M. T. Schmidt, P. Tham, and E. S. Yang, "Optically induced electromagnetic radiation from semiconductor surfaces," *Appl. Phys. Lett.*, vol. 56, pp. 2228-2230, May 28, 1990.

[15] S. Gupta, M. Y. Frankel, J. A. Valdmanis, J.F. Whitaker, G. A. Mourou, F.W. Smith, and A.R. Calawa, "Subpicosecond carrier lifetime in GaAs grown by molecular beam epitaxy at low temperatures', Appl. Phys. Lett. 59, 3276 (1991).

[16] R. Heidemann, TH. Pfeiffer, and D. Jager, "Optoelectronically pulsed slot-line antennas," *Electron. Lett.*, vol. 19, pp. 316-317, Apr. 28, 1983.

[17] D. Liu and J. Qin, "Carrier dynamics of terahertz emission from low-temperature-grown GaAs," *Appl. Opt.*, vol. 42, no. 18, pp. 3678-3683, June 2003

[18] D. C. Look, "Molecular beam epitaxial GaAs grown at low temperature," *Thin Solid Films*, vol. 231, pp. 61-73, 1993.

[19] J.Zhang, Y.Hong, S.L. Braunstein and K.A.Shore.;" Terahertz pulse generation and detection with LT-GaAs photoconductive antenna", IEE Proc.-Optoelectron., Vol. 151, No.2, April 2004.

[20] Hanmin Zhao, Jung H.Hur, P. Hadizad, and martin A. Gunderson, "Avalanche Injection Model for the lock-on effect in photoconductive power switches', Department of Electrical Engineering-Electrophysics, University of Southern California, Los Angeles, CA 90098-0484, Nov. 2000

[21] K. Yee, "Numerical solution of initial boundary value problems involving Maxwell's equations in isotropic media", *IEEE Trans. Antennas. Propagat.*, vol 14, pp. 302-307, 1966.

[22] A. Taflove and S. C. Hagness, Computational Electrodynamics: The Finite-Difference Time-Domain Method, 3rd ed., Artech House Publishers, 2005.

[23] A. Dreyhaupt, S. Winnerl, T. Dekorsy, and M. Helm, "High-intensity terahertz radiation from a microstructured large-area photoconductor," *Appl. Phys. Lett.*, vol. 86, pp. 121114, 2005.

[24] S. El-Ghazaly, R. Joshi and R. Grondin, "Electromagnetic and transport considerations in subpicosecond photoconductive switch modeling", *IEEE Trans. Microwave Theory Tech.*, vol. 38, no. 5, pp. 629-637, May 1990.

[25] D. M. Caughey and R. E. Thomas, "Carrier mobilities in silicon empirically related to doping and field," *Proc. IEEE*, vol. 55, pp. 2192-2193, 1967.

[26] R. Luebbers, K. Kunz, M. Schneider, and F. Hunsberger, "A finite-difference time-domain near zone to far zone transformation", *IEEE Trans. Antennas. Propagat.*, vol. 39, no. 4, pp. 429-433, April 1991.

[27] D. D. Nolte, “Semi-insulating semiconductor heterostructures: Optoelectronic properties and applications,” *Appl. Phys. Rev.*, vol. 89, no. 9, pp. 6259-6289, May 1999.

[28] Naz. E. Islam, Edl Schamiloglu and Vassilios Kovanis; “Simulation Studies of High Gain Photoconductive Semiconductor Switches used in High Power Microwave Generation”; IEEE Transactions.

[29] P. F. Lindquist, "A model relating electrical properties and impurity concentrations in semi-insulating GaAs," Journal of Applied Physics, vol. 48, pp. 1262-1267, 1977.

[30] Islam N.E, Schamiloglu E, Mar A, Loubriel G.M, Zutavern F.;” Characteristics of Trap-filled Gallium Arsenide Photoconductive switches used in high gain pulsed power applications”, IEEE Trans.

[31] N. E. Islam, E.Schamiloglu, and C. B. Fleddermann “Characterization of a semi-insulating GaAs photoconductive semiconductor switch for ultrawide band high power microwave applications.

[32] Masahiko Tani, Shuji Matsuura, Kiyomi Sakai, and Shin-ichi Nakashima, Emission Characteristics of photoconductive antennas based on low-temperature –grown GaAs and semi-insulating GaAs”, Applied Optics, Vol.36, No.30, 20 October 1997

[33] Silvaco Int., Atlas User’s Manual, Available : www.silvaco.com

[34] “Femtosecond Response of a Freestanding LT-GaAs Photoconductive Switch’, LLE Review, volume 90.

[35] Arye Rosen and Fred Zutavern "High-Power optically activated solid-state switches", Norwood, 1994

[36] F.J. Zutavern, G.M. Loubriel, M.W. O'Malley, L.P. Shanwald, W.D. Helgerson, D.L. McLaughlin, and B.B. McKenzie, "Photoconductive Semiconductor Switch Experiments for Pulsed Power Applications," IEEE Trans. On Electron Devices, Vol. ED-37, No. 12, pp. 2472-2477, December 1990

[37] R.L. Druce, W. W. Hofer, K. L. Griffin, J. J. Yee, G. H. Khanaka, and M. D. Pocha, "Photoconductive Switching in Gallium Arsenide," UCRL 53868-91, available from the National Technical Information Service, US Department of commerce, 5285 Port Royal Road, Springfield, VA 22161

[38] R. P. Brinkman, K.H. Schoenbach, D.C. Stout, V.K. Lakdawala, G.A. Gerdin, and M. K. Kennedy, "The Lock-on Effect in Electron-Beam-Controlled Gallium Arsenide Switches," IEEE Trans. On Electron Devices, Vol. 38, No. 4, April 1991

[39] Phumin Kirawanich, S.Joe Yakura, Carl E.Baum, and Naz E.Islam, "Analyzing Enhanced Terahertz-Pulse Power and Frequency Using a Field-Carrier Transport approach", IEEE Antennas And Wireless Propagation Letters, Vol. 7, 2008

[40] M. O. Manasreh, D. C. Look, K.R. Evans, and C. E. Stutz, " Infrared absorption of deep defects in molecular-beam-epitaxial GaAs layers grown at 200^0 C. observation of an EL2-like defect

[41] J. K. Luo, H. Thomas, D. V. Morgan, and D. Westwood, "Thermal annealing effect in low temperature molecular beam epitaxy grown GaAs: Arsenic precipitation and the change of resistivity, Appl. Phys. Lett. 64, 3614 (1994)

[42] Schoenberg J. S. H., J. W. Burger, J. S. Tyo, M. D. Abdalla, M. C. Skipper, and W. R. Buchwald, IEEE Trans. Plasma Sci., Vol. 25, p. 327, 1997

[43] Van Rosebroeck W. and H.C. Casey Jr., 'Transport in relaxation semiconductors", Phys. Rev. B Vol. 5, no. 6, p. 2154, 1972

[44] Cavicchi B. T. and Haegel N. M., "Experimental evidence of relaxation phenomenon in high purity silicon", Phys. Rev. Lett., vol.63, p.195, 1989

[45] Phumin Kirawanich, Susumu J. Yakura, Member, and Naz E.Islam, "Study of High-Power Wideband Terahertz-Pulse Generation Using Integrated High-Speed Photoconductive Semiconductor Switches", IEEE Transactions On Plasma Science, Vol. 37, No.1, January 2009

[46] Haegel N. M., "Relaxation Semiconductors: In theory and in practice", Phys. A, vol. 53, p. 1, 1991

[47] Holmes D. E., R. T. Chen, Kenneth R. Elliott, C. G. Kirkpatrick, and Phil Won Yu, "Compensation Mechanism in Liquid Encapsulated Czochralski GaAs : Importance of Melt Stoichiometry", IEEE trans. On Electron Devices, Vol. ED-29, No. 7, July 1982

[48] Islam, N. E.; Schamiloglu, E.; Fleddermann, C.B., Schoenberg, J.S.H.; Josh, R.P, "Improved hold-off characteristics of Gallium Arsenide photoconductive switches used in high power applications", Vol.1, Intl. Conference on Plasma Science, June 1999

[49] Zutavern F. J., G. M. Loubriel, M. W. O'Malley, L. P. Schnwald, D. L. McLaughlin, "Recovery of high-field GaAs photoconductive semiconductor switches", IEEE Electron Devices., Vol 38, no. 4, pp. 696-700, Apr. 1991

[50] Chang M. F., C. P. Lee, L. D. Hou, R. P. Vahrenkamp, and C.G. Kirkpatrick, "Mechanism of surface conduction in semi-insulating GaAs", Appl. Phys. Lett., Vol. 44, no.9, pp.869-871, May 1984

[51] Partain L., D. Day, and R. Powell, "Metastable impact ionization of traps model for lock-on in GaAs photoconductive switches", J. Appl. Phys., vol. 74, no .1, pp. 335-340, July 1993

[52] Kambour and S.Kang, " Steady-State Properties of Lock-on Current Filaments in GaAs", IEEE Trans. On Plasma Sci., vol. 28, no. 5, pp. 1497-1499, Oct. 2000

[53] Murray A. Lampert and Peter Mark, "Current Injection Solids." Academic Press, New York, 1970

[54] Y. C. Shen, P. C. Upadhya, E. H. Linfield, H. E. Beere, and A .G. Davies, " Ultrabraodband terahertz radiation from low-temperature-grown GaAs photoconductive emitters" Applied Physics Letters, Vol. 83, Number 15, October 2003

[55] F. W. Smith, A. R. Calawa, C–L. Chen, G. W. Turner, M. C. Finn, L. J. Mahoney, and A. R. Calawa, "Sidegating reduction for GaAs integrated circuits by using a new buffer layer", Int. Electron Device Meeting, Techn. Digest (IEEE Cat. No. 88-CH2528-8), 839 (1988).

[56] M. Kaminska, Z. Lilienthal- Weber, T. George, J. B. Kortright, F. W. Smith, B. Y. Tsaur, and A. R. Calawa, "Structural properties of As-rich GaAs grown by molecular beam epitaxy at low temperatures", Appl. Phys. Lett. 54, 1881 (1989).

APPENDIX

Simulation code for SI-GaAs PCSS and LT-GaAs PCSS

#DEVEDIT VERSION=2.8.7.R # FILE WRITTEN WED APR 13 2011 13:20:23 GMT-5 (CDT)

go devedit

work.area x1=0 y1=-10 x2=50 y2=50

devedit 2.8.7.R (Fri Apr 4 17:46:09 PDT 2008)

libMeshBuild 1.24.5 (Fri Apr 4 17:38:34 PDT 2008)

libSSS 2.6.3 (Fri Apr 4 17:26:34 PDT 2008)

libSVC_Misc 1.28.3 (Thu Mar 6 15:35:06 PST 2008)

libsflm 7.4.16 (Mon Mar 10 16:31:43 PDT 2008)

libSDB 1.10.10 (Fri Mar 28 17:23:21 PDT 2008)

libGeometry 1.28.4 (Thu Mar 6 15:34:57 PST 2008)

libCardDeck 1.30.4 (Thu Mar 6 15:32:16 PST 2008)

libDW_Set 1.28.3 (Mon Mar 3 19:39:47 PST 2008)

libSvcFile 1.12.4 (Thu Mar 6 15:37:02 PST 2008)

libsstl 1.8.7 (Thu Mar 6 15:37:39 PST 2008)

libDW_Misc 1.38.5 (Thu Mar 6 15:27:39 PST 2008)

libQSilCore 1.2.2 (Wed Aug 30 19:34:57 PDT 2006)

liberror 1.0.6 (Wed Aug 30 19:34:52 PDT 2006)

libDW_Version 3.2.0 (Wed Aug 30 19:34:31 PDT 2006)

```
region reg=1 mat=GaAs color=0x7f00 pattern=0x9 \
        polygon="0,0 20,0 30,0 50,0 50,50 0,50"
#CONSTR.MESH REGION=1 DEFAULT

region reg=2 name=cathode mat=Aluminum elec.id=1 work.func=0 color=0xffc8c8 pattern=0x7 \
        polygon="0,-1 20,-1 20,0 0,0"
#constr.mesh region=2 default
region reg=3 name=anode mat=Aluminum elec.id=2 work.func=0 color=0xffc8c8 pattern=0x7 \
        polygon="50,0 30,0 30,-1 50,-1"
#constr.mesh region=3 default
# SET MESHING PARAMETERS
#base.mesh height=10 width=10
#bound.cond !apply max.slope=30 max.ratio=100 rnd.unit=0.001 line.straightening=1 align.points when=automatic
#imp.refine min.spacing=0.02
#constr.mesh max.angle=90 max.ratio=300 max.height=1000 \
        max.width=1000 min.height=0.0001 min.width=0.0001
#CONSTR.MESH TYPE=SEMICONDUCTOR DEFAULT
#CONSTR.MESH TYPE=INSULATOR DEFAULT
#CONSTR.MESH TYPE=METAL DEFAULT
#CONSTR.MESH TYPE=OTHER DEFAULT
```

```
#constr.mesh region=1 default

#constr.mesh region=2 default

#constr.mesh region=3 default

Mesh Mode=MeshBuild

refine mode=both x1=0.28 y1=0.1 x2=49.73 y2=49.6

refine mode=both x1=0.19 y1=0.2 x2=49.82 y2=49.4

base.mesh height=10 width=10

bound.cond !apply max.slope=30 max.ratio=100 rnd.unit=0.001 line.straightening=1

align.Points when=automatic

go atlas

#ADDED IMPURITY

doping uniform p.type conc=2.5e15 direction=y x.min=0 x.max=50 \

  y.min=0 y.max=50

#BEAM

beam num=1 x.origin=25 y.origin=-25 angle=90.0 wavelength=.780   \

min.window=-25 max.window=50

#Defined Models

models material= GaAs conmob fldmob srh auger numcarr=2 bbt.std\

      print

#Impace Ionization

impact material = GaAs selb length.rel

#LIFETIMES OF HOLES AND ELECTRONS

material region=1 name=GaAs  taup0=4e-13 taun0=1e-13
```

```
#MOBILITY
mobility ymaxn.watt=0.06 xminn.watt=30 xmaxn.watt=50 \
 ymaxp.watt=0.06 xminp.watt=30 xmaxp.watt=50
#CONTACT RESISTANCE
contact name=anode resistance=45
contact name=cathode resistance=45
log outfile=IV250lt.log
solve init
solve vanode=1    vstep=1   vfinal=250 name=anode
save outf=ltGaAs250.str
tonyplot ltGaAs250.str
tonyplot IV250lt.log
log outf=ltLas250.log
output     e.field j.electron j.hole j.conduc j.total ex.field ey.field \
      flowlines charge recomb j.disp impact tot.doping e.mobility \
       e.velocity h.mobility h.velocity
solve B1=0.0 ramptime=3e-15 tstop=200e-15 tstep=1e-13
solve B1=5e7 ramptime=200e-15 tstop=280e-15 tstep=1e-13
save outf=lt250LasGaAson.str
output     e.field j.electron j.hole j.conduc j.total ex.field ey.field \
      flowlines charge recomb j.disp impact tot.doping e.mobility \
       e.velocity h.mobility h.velocity
solve B1=0.0 ramptime=280e-15 tstop=8000e-15 tstep=1e-13
```

```
output      e.field j.electron j.hole j.conduc j.total ex.field ey.field \
        flowlines charge recomb j.disp impact tot.doping e.mobility \
         e.velocity h.mobility h.velocity
tonyplot ltLas250.log
quit
```